

Chemical composition of carbon-rich, very metal-poor subgiant LP625-44 observed with the Subaru/HDS*

Wako AOKI¹, Hiroyasu ANDO², Satoshi HONDA¹, Masanori IYE¹, Hideyuki IZUMIURA³,
Toshitaka KAJINO¹, Eiji KAMBE⁴, Satoshi KAWANOMOTO¹, Kunio NOGUCHI¹,
Kiichi OKITA¹, Kozo SADAKANE⁵, Bun'ei SATO^{3,6}, Ian SHELTON², Masahide TAKADA-HIDAI⁷,
Yoichi TAKEDA⁸, Etsuji WATANABE³ and Michitoshi YOSHIDA³

¹*National Astronomical Observatory, Mitaka, Tokyo, 181-8588*

aoki.wako@nao.ac.jp

²*Subaru Telescope, National Astronomical Observatory of Japan,
650 North Aohoku Place, Hilo, HI96720, USA*

³*Okayama Astrophysical Observatory, National Astronomical Observatory of Japan,
Kamogata-cho, Okayama, 719-0232*

⁴*Department of Earth and Ocean Sciences, National Defense Academy,
Hashirimizu 1-10-20, Yokosuka, Kanagawa 239-8686*

⁵*Astronomical Institute, Osaka Kyoiku University,
Kashiwara-shi, Osaka, 582-8582*

⁶*Department of Astronomy, School of Science, University of Tokyo,
Bunkyo-ku, Tokyo 113-0033*

⁷*Liberal Arts Education Center, Tokai University, 1117 Kitakaname,
Hiratsuka-shi, Kanagawa, 259-1292*

⁸*Komazawa University, Komazawa, Setagaya, Tokyo, 154-8525*

(Received 0 0; accepted 0 0)

Abstract

We have obtained a high resolution ($R \sim 90,000$) spectrum of the carbon- and s -process-element-rich, very metal-poor ($[\text{Fe}/\text{H}] = -2.7$) subgiant LP 625-44, as well as that of HD 140283 (a metal-poor subgiant with normal abundance ratio) for comparison, with the High Dispersion Spectrograph (HDS) for the Subaru Telescope for detailed abundance study. The spectrum covers 3400-7800Å and enables us to study important spectral lines which had not been detected in the previous works. We found significant overabundances in some light elements, in addition to carbon and nitrogen for which large enhancements were already known. The oxygen abundance derived from the O I triplet around 7770Å is uncertain, but the excess of oxygen in LP 625-44 seems remarkable (perhaps by nearly a factor 10), in comparison with that of HD 140283 derived from the same lines. The Na enhancement in LP 625-44

is by about a factor 50, suggesting hydrogen burning in the ^{22}Ne -rich layer in an asymptotic giant branch star which produces the abundance pattern of this object. In our new spectrum of LP 625-44, the Pb I $\lambda 3683\text{\AA}$ line has been detected, as well as the Pb I $\lambda 4057\text{\AA}$ line which has already been studied, confirming the Pb abundance ($\log \epsilon(\text{Pb}) \sim 1.9$) derived by the previous work. The abundance ratio of *s*-process elements at the second peak (e.g., La, Ce and Nd) to that at the third peak (Pb) in LP 625-44 is significantly higher (by a factor 5) than that in other three *s*-process element-rich objects recently studied by van Eck et al.. Recent theoretical works have modeled the *s*-process nucleosynthesis in the radiative layer of asymptotic giant branch stars in the inter-pulse phase, and the above results means that these processes produced a large scatter in the abundance ratios. Another possibility is that different processes (e.g., *s*-process nucleosynthesis during thermal pulses) have contributed to heavy elements in the early Galaxy.

Key words: nuclear reactions, nucleosynthesis, abundances – stars: abundances – stars: AGB and post-AGB – stars: carbon – stars: Population II

1. Introduction

The chemical composition of very metal-poor stars (e.g., $[\text{Fe}/\text{H}] < -2.5$) is believed to be determined by a small number of nucleosynthesis processes preceding the formation of these objects. Abundance studies for these objects in the past decade have provided rich information for our understanding of individual nucleosynthesis processes in the early Galaxy (000 [cite]cite.mcwilliam95McWilliam et al. (1995); 000 [cite]cite.ryan96Ryan, Norris & Beers (1996)).

The very metal-poor ($[\text{Fe}/\text{H}] \sim -2.7$) subgiant LP 625-44 shows extremely large over-abundances of carbon, nitrogen and neutron-capture elements (000 [cite]cite.norris97aNorris, Ryan & Beers (1997)). This abundance property indicates the nucleosynthesis products in the asymptotic giant branch (AGB) stage of low-mass or intermediate-mass stars ($M = 1 \sim 8M_{\odot}$, Iben & Renzini 1983). Since the evolutionary time-scale of these objects is long (100M \sim 1G year), the abundance pattern of LP 625-44 is not considered to originate in the gas cloud from which this object formed, but to reflect the yields of nucleosynthesis after this object has formed. One possible model to explain the abundances of this object is that involving mass transfer from a carbon-enhanced AGB star (one that has since evolved to the white dwarf stage and cannot now be seen) to its lower-mass companion, which is now observed as a carbon-rich object like LP625-44. The binarity of this object was confirmed by radial-velocity monitoring

* Based on data collected at Subaru Telescope, which is operated by the National Astronomical Observatory of Japan.

(000 [cite]cite.aoki00Aoki et al.(2000)), strongly supporting the above mass transfer scenario. This means that the nucleosynthesis process even in low-mass and intermediate-mass stars can also be studied by abundance analyses of such special metal-poor objects. The abundance pattern of the heavy neutron capture elements in LP 625-44 agrees well with that of solar system *s*-process elements (000 [cite]cite.aoki00Aoki et al.(2000)). Detailed abundance study of this star will give a strong constraint on *s*-process nucleosynthesis at low metallicity and AGB evolution in the early Galaxy.

Recent modeling of AGB stars by te]cite.straniero95Straniero et al. (1995) ([cite]cite.straniero95Straniero et al. (1995)) showed that neutron capture mainly occurs, not in the convective He shell *during* a thermal pulse, but in the radiative state *between* two given pulses. In this model the density distribution of the ^{13}C -rich layer (referred to as the ^{13}C pocket), which provides neutrons for the *s*-process, is taken as a free parameter. The yields of neutron-capture elements have been systematically calculated based on the stellar models by te]cite.gallino98Gallino et al. (1998) ([cite]cite.gallino98Gallino et al. (1998)), who succeeded in reproducing at least the main component of the solar-system *s*-process elements. The *s*-process nucleosynthesis in the inter-pulse phases was also studied by Goriely & Mowlavi (2000), who model the mixing process via a diffusion mechanism. On the other hand, quite recently, te]cite.iwamoto02Iwamoto et al. (2002) ([cite]cite.iwamoto02Iwamoto et al. (2002)) have found theoretically that the proton mixing into helium burning layer occurs *during* thermal pulses *only in* very metal-deficient ($[\text{Fe}/\text{H}] \leq -2.5$) AGB stars (see section 4.3 for details). This model predicts a large neutron exposure, and a different *s*-process abundance pattern from those of the standard model of te]cite.gallino98Gallino et al. (1998) ([cite]cite.gallino98Gallino et al. (1998)) and te]cite.goriely00Goriely & Mowlavi (2000) ([cite]cite.goriely00Goriely & Mowlavi (2000)).

One issue to be studied for LP 625-44 is the lead (Pb) abundance. The detection of Pb in LP 625-44 by te]cite.aoki00Aoki et al.(2000) ([cite]cite.aoki00Aoki et al.(2000)) enables a comparison of the abundance pattern from Sr ($Z = 38$) to Pb ($Z = 82$) with predictions of AGB models. The Pb I line ($\lambda 4057$) used in the above study has recently been detected in other three objects by te]cite.vaneck01van Eck et al. (2001) ([cite]cite.vaneck01van Eck et al. (2001)). An important result of the work is that the Pb of these three objects are much more abundant than the elements with $Z \sim 60$ (e.g., Ce and Nd), and the abundance ratios like Ce/Pb and Nd/Pb are significantly lower than those of LP 625-44. This implies a large scatter in these abundance ratios which represent the production ratio of the elements at the second- to the third-peaks for *s*-process at low metallicity. Despite the importance of its Pb abundance, the abundance analysis for Pb in LP 625-44 relies only on the $\lambda 4057\text{\AA}$ line (the situation is the same for the other three objects). Confirmation of the Pb abundance by other lines is strongly desired.

Another issue concerning the chemical composition of LP 625-44 is the abundances

of light elements. *S*-process nucleosynthesis is dependent on the conditions of the burning layer in AGB stars, which may be investigated by the resulting abundances of carbon, nitrogen, oxygen and other light elements. A large excess of carbon and nitrogen, and moderate enhancement of magnesium have been revealed by te]cite.norris97aNorris, Ryan & Beers (1997) ([cite]cite.norris97aNorris, Ryan & Beers (1997)) and te]cite.aoki00Aoki et al.(2000) ([cite]cite.aoki00Aoki et al.(2000)). Other elements like oxygen (O) and sodium (Na) are also useful to assess the nucleosynthesis processes which have contributed to the chemical nature of LP 625-44.

For the study mentioned above, we obtained high resolution spectrum of LP 625-44 with the High Dispersion Spectrograph (HDS) of the 8.2m Subaru Telescope. The HDS is an échelle spectrograph for the optical wavelength region (3000-10,000Å) located at one of the Nasmyth foci of the telescope. HDS successfully achieved its first-light in early July, 2000. Our spectra have been acquired in the first and second test observing runs for HDS, and show the quality of the spectrograph, though some minor problems still existed in the early phases of performance verification.

In this paper, we study the characteristics of the abundances of the carbon- and *s*-process-element-rich star LP 625-44, comparing with the abundances of the metal-poor subgiant (with normal abundance ratios) HD140283, which was also observed with similar setups of HDS. We describe the observation, data reduction and calibration in some detail in section 2. The equivalent widths, intrinsic line widths and radial velocities are measured in that section. In section 3, the analysis for absorption lines of the *s*-process elements including Pb I λ 3683 and those of some light elements are described. We discuss the interpretation of the large excesses of some light elements including O and Na, and the variation of abundance patterns for the *s*-process elements in section 4.

2. Observation and Measurements

2.1. Observation with Subaru HDS

The observation has been made with Subaru/HDS in July and August, 2000. The échelle grating of this instrument is a mosaic of two 31.6 gr/mm gratings, and the dispersion is 1 Å/mm at 4300 Å. The detector is a mosaic of two 4k×2k EEV CCD's with 13.5μm pixels. We adopted a 0.4 arcsec (0.2 mm) slit width which enables us to get spectra with resolution about 90,000 by about 3.5 pixels sampling. The high resolving power and high sampling rate are valuable in the study of the elemental lines affected by the isotope shifts or by blending with other atomic or molecular lines.

We observed our two objects with both standard blue and red setups of the spectrograph as given in Table 1. Another spectrum was also obtained with the UV setup (3100-4500 Å) for HD140283. It should be noted that the central wavelength range (one order or two) of each

region cannot be observed due to the gap (~ 1.1 mm) between the two CCD's. While the free spectral range is completely covered by the blue setup, that is not the case in the wavelength region longer than 7200 \AA in the red setup. A short-wavelength-cutoff filter (SC46) was used in the observations of red spectra.

In the observing runs in July and August 2000, the atmospheric dispersion compensator (ADC) had not yet been installed. The image rotators were used because the target acquisition and guiding without image rotators had not yet been tested. In particular, the blue spectrum ($3400\text{-}5100 \text{ \AA}$) of HD140283 was obtained using the image rotator for the red setup, because the blue one was not available in the July run. We adopted the August data as the blue spectrum ($<4500 \text{ \AA}$) for HD140283. Using the image rotator, the slit image on the sky was fixed to the pole direction, instead of the zenith direction, due to the requirement of guiding at that time. Therefore the loss of light was significant in the short wavelength region in which the atmospheric differential dispersion is quite large. This limit in the observation resulted in the lower quality of the spectra for the short wavelength region ($\lambda < 3300 \text{ \AA}$).

We note that the ADC for the Nasmyth focus of the Subaru telescope was installed in January 2001. The throughput is better than that of image rotators for $\lambda > 3500 \text{ \AA}$, and observing efficiency has improved compared to that in the observing runs when we obtained the data studied in this work. Guiding without image rotators also became available after our observing runs.

For flat fielding of the CCD data, we obtained Halogen lamp data (hereafter flat data) with the same setup as that for object frames. However, we found in the July data that there was a significant disagreement of the continuum profile and the fringe pattern between the object spectrum and the flat one. The disagreement of the continuum profile is not serious for our abundance study because the analysis is usually made for normalized spectra, but the difference of the fringe pattern, which is remarkable in the red and near infrared ranges, directly affects our study of weak absorption features. By an investigation after the July run, we found that this problem was mainly due to the mis-alignment of the calibration system. In the August run, we fixed the problem and obtained the flat data again with the same setup as in the July run. Using the new flat data, the calibration quality has significantly improved, and the fringes have almost disappeared in our spectra.¹ We note that the stability of the detector system including temperature control is fairly good, and the flat data obtained in different observing runs are applicable to data with the quality achieved in our study.

¹ There is still a problem of fringes and continuum profile in HDS data, but that is not due to the problem of the calibration system, but may be due to the fluctuation in the angle of the incident beam from the telescope.

2.2. Data reduction

In the present data acquisition system of HDS, two FITS formatted CCD data files are produced for one exposure corresponding to the two CCD's. These two files are reduced separately in this work. Standard data reduction using the IRAF² *echelle* package was applied to each frame following the procedures mentioned below.

HDS data frames include a so-called “over-scan region” which represents the bias level of the frame. Though the time variation of the bias level is not large in HDS (1-2 e⁻), we corrected the bias level by subtracting the average of the counts in the over-scan region for each frame. Since there are two output points for each CCD, and the gains (conversion factors) are slightly different between them, the conversion from ADU to the number of electrons was made corresponding to the output point.

The dark current of the CCD is about 1e⁻ per hour, and is negligible in this study. However, some emission inside the Nasmyth enclosure or leakage of light from the outside about 10 e⁻ per hour is known. This makes an almost homogeneous background in our object frames, and can be corrected by the background subtraction mentioned below. For this reason we have not acquired so-called dark frames in our observing runs.

Most cosmic-ray noise is excluded by comparing frames obtained by the same setup of the instrument. When more than three frames were acquired with the same setup, we replaced the count of a pixel by the median value of the all frames if the count of the individual frames is significantly higher than that of the median frame. When only two frames are available for the identical setup, we made a difference of the two frames, and replace the count of a pixel by that in another frame if the difference is significantly larger or smaller than zero.

There are several distinctive so-called bad (or hot) columns in the CCD's, which align with the échelle dispersion direction. We excluded the wavelength regions of the spectra affected by these columns in the present analysis.

The background subtraction was done by the '*apscatter*' routine of IRAF. The background level is about 2% of the stellar flux at 4000Å for LP625-44, and higher at shorter wavelength due to the decrease of the stellar flux. This background level is explained by reflections of the stellar light at the surface of the CCD and the field flattener lens just before the CCD. A comparison of the count level on the slit image and that of the inter-order region has shown that the sky contamination is negligible for our objects.

As mentioned in the previous subsection, the calibration system was re-aligned after the July run, and the quality of flat-fielding has improved. However, the fringes in the longest wavelength range ($\sim 7800\text{\AA}$) cannot necessarily be canceled out by flat fielding, because of the small variation of the fringe pattern amongst the object data. Fringes can be the most severe

² IRAF is distributed by the National Optical Astronomy Observatories, which is operated by the Association of Universities for Research in Astronomy, Inc. under cooperative agreement with the National Science Foundation.

source of noise in the spectrum for the long wavelength range.

The wavelength calibration was done using the Th-Ar spectra obtained before and/or after the observations of the targets. The measured rms wavelength error of the weak Th lines is less than 0.01Å. By the measurement of the FWHM of weak Th lines, we confirmed the spectral resolution as about 90,000.

The CCD covers the spectrum of each order much wider than the free spectral range in the UV-blue region. We trimmed the wavelength range where the count level is too low (typically lower than 1/4 of the peak of the échelle blaze profile) from the spectrum of each order to reduce the noise included in the region with low-count level.

For continuum specification, we first made blaze profiles of individual échelle orders using the flat data. The stellar spectra were divided by these blaze profiles, and the continuum was traced using IRAF '*continuum*' routine. The continuum specification is still difficult for the regions around broad absorption lines (e.g., Balmer lines) and strong molecular bands (e.g., CH G-band), but they are not important for the present analysis focusing on rather weak lines.

The S/N ratio of each spectrum, simply estimated from the count level, is given in the last column of Table 1. This value is the S/N ratio per pixel (0.012Å at 4000Å and 0.018Å at 6000Å) at the peak of the échelle blaze profile. The S/N ratio at the edge of the échelle blaze function is lower than the center. However, the free spectral range is well covered for most regions, and the S/N ratio is not severely dependent on the line position in the échelle order after combining the spectra for neighboring orders.

2.3. *Measurement of equivalent widths*

For the standard analysis which was applied to most elements, equivalent widths were measured by fitting Gaussian profiles to the absorption lines. We excluded lines which may be significantly affected by other absorption lines. The blending with other atomic or molecular lines was checked using the atomic line list by te]cite.kurucz95Kurucz & Bell (1995) ([cite]cite.kurucz95Kurucz & Bell (1995)) and molecular line lists of CH, CN and C₂ (000 [cite]cite.aoki01Aoki et al. (2001)). The spectral lines which are too broad compared to the lines with similar strength are also excluded to avoid possible blending with unknown line absorption. The line list including the equivalent widths measured is given in Table 3.

In Figure 1, the equivalent widths of Fe I measured in the present work are compared with those of te]cite.norris96Norris, Ryan & Beers (1996) ([cite]cite.norris96Norris, Ryan & Beers (1996)) and te]cite.king98King et al. (1998) ([cite]cite.king98King et al. (1998)) for HD140283, and those of te]cite.aoki00Aoki et al.(2000) ([cite]cite.aoki00Aoki et al.(2000)) for LP625-44. The agreement is fairly good between our measurement and that of te]cite.king98King et al. (1998) ([cite]cite.king98King et al. (1998)). The agreement between our data and those by te]cite.norris96Norris, Ryan & Beers (1996) ([cite]cite.norris96Norris, Ryan & Beers (1996)) is also good for weak lines which are important for abundance determination, though our

equivalent widths of strong lines are slightly ($\sim 5\%$) smaller than theirs. On the other hand, the dispersion in the diagram for LP 625-44 is larger than the dispersion in those for HD 140283. This should be due to the lower S/N ratios of the LP625-44 spectrum than that of the HD140283 one in both studies, and may also be due to the effect of unidentified blending, because the lines are very crowded in LP 625-44 due to the overabundances of carbon, nitrogen and neutron-capture elements.

2.4. *Intrinsic line widths*

Thanks to the high resolving power of HDS ($\sim 3.5 \text{ km s}^{-1}$), the instrumental line broadening is sometimes smaller than the intrinsic widths of metal lines due to the motion of the photospheric gases (macro-turbulence) and/or stellar rotation. We plot the widths of Fe I lines observed against their central depths in Figure 2. The width in the figure indicates the Gaussian dispersion in velocity units (km s^{-1}) converted from the FWHM and corrected for instrumental broadening for which we assumed a Gaussian profile. We excluded the lines whose central depths are shallower than 0.1 because their quality is not good. Then we determined the optically thin limit of the line width by extrapolating the plots to zero central depth. This thin limit can be interpreted as the intrinsic line width.

The thermal broadening for our objects ($T_{\text{eff}} \sim 5500\text{K}$) is about 1.8 km s^{-1} , and the micro-turbulent velocity is 1.2 km s^{-1} (see section 3). Correcting for these broadening, the macroscopic broadening is estimated to be 5.5 and 7.4 km s^{-1} for HD140283 and LP625-44, respectively. We expect that the rotation of these old subgiants is slow, and the broadening represents the macro-turbulence in the atmosphere.

However, as found in the lower panel of Figure 2 for LP625-44, the scatter in the widths of weak lines is large, and there seems to be an influence of blending on some weak lines. Since this object shows remarkable overabundances of carbon, nitrogen and neutron-capture elements, blending with absorption lines of molecules and heavy elements is a significant problem. We tried an independent estimation of the line broadening for a rather strong and clean Fe I line ($\lambda 4143.87$) by fitting a synthetic spectrum (Figure 3). The stellar parameters used for the calculation are given in next section. We assumed a single Gaussian broadening here. This assumption is expected to be enough to estimate the broadening for the following analysis, though that may not represent the broadening process of the real atmosphere. This analysis showed that line broadening of 7.4 km s^{-1} seems to be an overestimate, but about 6.5 km s^{-1} is acceptable. We adopted the later as the macro-turbulence of LP625-44.

We estimate here for completeness the effect of blending on measurement of equivalent widths. If the discrepancy in the measured macro-turbulence from Figure 2 and that from the Fe II $\lambda 4143$ line is due to blending with other lines, that also results in the overestimate of equivalent widths for the weak Fe I lines used in the abundance analysis, and then the derived iron abundances. The effect is about 15% (0.06 dex) for some weak lines, and that does not

make large impact on the abundance determination.

2.5. Measurement of radial velocity

Variation of radial velocity has been detected for LP 625-44 by te]cite.norris97aNorris, Ryan & Beers (1997) ([cite]cite.norris97aNorris, Ryan & Beers (1997)) and te]cite.aoki00Aoki et al.(2000) ([cite]cite.aoki00Aoki et al.(2000)). This fact indicates the binarity, and strongly supports the mass transfer scenario as an explanation for the overabundances of carbon and *s*-process elements in this star. Since one period of the variation has not yet been covered in the monitoring, further measurements of radial velocity are indispensable to determine the orbital parameters for this object.

For the measurement of radial velocity, we selected clean Fe I lines in each spectrum, and measured the line position by fitting Gaussian profiles, and then derived the heliocentric velocity. Results are given in Table 2, along with the standard error in each measurement and the Julian Day (JD) of the observation. We note that the Th-Ar comparison data were not acquired before nor after the HD140283 observing on 18 August run, so a reliable radial velocity could not be derived from that spectrum.

The results from the two measurements for HD 140283 agrees very well. No variation of radial velocity is known for this object, and our results are reasonable. The radial velocities of LP 625-44 (30.2 and 30.9 km⁻¹) are almost consistent with the result (30.0 km⁻¹) for JD=2451569.8 (000 [cite]cite.aoki00Aoki et al.(2000)). The variation of radial velocity for this object is expected to be small for about 200 days, and the results are also reasonable.

3. Abundance analysis and Results

An abundance analysis using model atmospheres in the ATLAS grid of te]cite.kurucz93aKurucz (1993) ([cite]cite.kurucz93aKurucz (1993)) was made for our two metal-poor objects. While a standard analysis based on equivalent widths was carried out for most elements, a spectrum synthesis technique was applied to molecular bands (CH, CN and C₂) and atomic lines which are affected by blending and/or line splitting (hyperfine splitting and isotope shifts). In this section, we describe the procedures and results of the abundance analysis.

3.1. Stellar parameters

The parameters of model atmospheres used in the abundance analysis are effective temperature (T_{eff}), surface gravity (g), micro-turbulent velocity (v_{micro}), and metallicity ([Fe/H] is adopted as metallicity). Once these parameters are given, the equivalent width is calculated for assumed elemental abundances for each line whose lower excitation potential (χ) and transition probability (g_f) are known. We determine the abundance from the comparison of the calculated equivalent widths with observed ones. There are other parameters of line broadening

like macro-turbulence for the spectrum synthesis method.

The effective temperatures have been determined by te]cite.norris97aNorris, Ryan & Beers (1997) ([cite]cite.norris97aNorris, Ryan & Beers (1997)) and te]cite.ryan96Ryan, Norris & Beers (1996) ([cite]cite.ryan96Ryan, Norris & Beers (1996)) for LP625-44 (5500K) and HD140283 (5750K), respectively. These are based on their color ($R - I$), and we adopted these values in this analysis.

For a check of the effective temperature, we investigated the correlation between the lower excitation potential and the resulting abundances for Fe I lines (Figure 4). The middle panel of this figure shows the correlation for the effective temperature adopted in this analysis. Though the abundances resulting from high excitation lines ($\chi \sim 4$ eV) are higher than those from low excitation ($\chi \sim 0$ eV), the discrepancy is not significant (~ 0.2 dex).

The top and bottom panels show the same ones for $T_{\text{eff}} = 5250$ and 5750 K, respectively. It should be noted that the abundances are derived using v_{micro} re-determined for each case, instead of the v_{micro} derived in the analysis for $T_{\text{eff}} = 5500$ K. The dependence of resulting abundances on the lower excitation potential slightly changes, but the effect of the change of effective temperature is not large. This is probably because the effect of effective temperature is partly canceled out by the re-determination of v_{micro} , because the equivalent width is strongly dependent on the excitation potential of the line (lines with low excitation potential are usually strong, while high excitation lines are usually weak). This implies that the correlation between excitation and resulting abundance does not give a strong constraint on the determination of effective temperature for this object. We note there is another difficulty in the estimation of effective temperatures from the relation between excitation and resulting abundance due to the uncertainty in the treatment of damping (000 [cite]cite.ryan98Ryan (1998)).

The surface gravity was determined to obtain ionization balance between Fe I and Fe II lines, and also between Ti I/Ti II. The final derived gravities are $\log g = 3.3$ and 2.5 for HD 140283 and LP 625-44, respectively. The micro-turbulent velocities were determined from the Fe I lines by demanding no dependence of derived abundance on equivalent widths. An example is shown in Figure 5. The result is 1.2 km s^{-1} in both objects. These values agree rather well with those derived by previous works (000 [cite]cite.ryan96Ryan, Norris & Beers (1996); 000 [cite]cite.aoki00Aoki et al.(2000)).

The random errors in standard analysis for Fe and Ti, which include errors in equivalent width measurements and uncertainties of gf -values, are about 0.1 dex or smaller. These errors result in the uncertainties of about 0.3 dex in $\log g$ and of 0.3 km s^{-1} in micro-turbulent velocities. We estimate the errors of the abundances caused by the uncertainties in stellar parameters in section 3.4.

The surface gravity of HD 140283 was measured by te]cite.fuhrmann98Fuhrmann (1998) ([cite]cite.fuhrmann98Fuhrmann (1998)) based on the Hipparcos parallaxes. Their result is $\log g = 3.7 \pm 0.1$, rather higher than the value derived from the ionization bal-

ance by some spectroscopic studies including our present work. The difference between the $\log g$ of te]cite.fuhrmann98Fuhrmann (1998) ([cite]cite.fuhrmann98Fuhrmann (1998)) and ours (0.4 dex) is comparable to the uncertainty of $\log g$ in this work (0.3 dex), but the discrepancy may be due to the non-LTE effect, as suggested by te]cite.fuhrmann98Fuhrmann (1998) ([cite]cite.fuhrmann98Fuhrmann (1998)).

3.2. Neutron-capture elements

The neutron capture elements of LP 625-44 were studied by te]cite.aoki01Aoki et al. (2001) ([cite]cite.aoki01Aoki et al. (2001)) in detail. We re-analyzed the abundances for most elements using the line lists produced by that work for new spectrum. The effect of hyperfine splitting and isotope shifts were included for the lines of Ba, La, Pr, Nd, Sm, Eu and Pb. The effect seems very small in Ce lines, and that was neglected: see te]cite.aoki01Aoki et al. (2001) ([cite]cite.aoki01Aoki et al. (2001)) for details of the line lists and analysis. Here we discuss some new lines of neutron capture elements which were not studied by the previous work. We inspected carefully the spectrum of HD140283, but could not find distinct absorption feature of neutron capture elements except for Sr, Y, Zr and Ba.

3.2.1. Pb I lines

Since the Pb abundance derived by te]cite.aoki00Aoki et al.(2000) ([cite]cite.aoki00Aoki et al.(2000)) and te]cite.aoki01Aoki et al. (2001) ([cite]cite.aoki01Aoki et al. (2001)) is based on the $\lambda 4057$ line alone, confirmation of the abundance from other lines is desirable. In the solar spectrum, four Pb I lines have been identified at 3639.5, 3683.4, 3739.9 and 4057.8 Å (000 [cite]cite.youssef89Youssef & Khalil (1989)). Two of them ($\lambda 3683.4$ and $\lambda 4057.8$) are found in our new spectrum of LP 625-44. Figure 6 shows the observed spectrum at the wavelength of these two lines with the synthetic spectra. In the calculation of the spectra, the effects of isotope (^{204}Pb , ^{206}Pb , ^{207}Pb and ^{208}Pb) shifts and hyperfine splitting for ^{207}Pb are taken into account. The line positions taken from te]cite.manning50Manning, Anderson & Watson (1950) ([cite]cite.manning50Manning, Anderson & Watson (1950)) are shown for each component in the figure. We assumed the solar system isotope ratio for Pb in this analysis. The upper panel of this figure shows the same line ($\lambda 4057.8$) at the top panel of Figure 2 in te]cite.aoki01Aoki et al. (2001) ([cite]cite.aoki01Aoki et al. (2001)), and the resulting abundance of this work ($\log \epsilon(\text{Pb}) = +1.9$) agrees with the previous result. One advantage of our spectrum is its higher spectral resolution and finer sampling. That makes it possible to investigate the effect of hyperfine structure and isotope shifts on the line profile which do not clearly appear in the spectrum studied by the previous work. The dashed line in Figure 6 indicates the synthetic spectrum calculated by single-line approximation for $\log \epsilon(\text{Pb}) = +1.9$. Even if a higher Pb abundance is assumed, the single-line approximation can never reproduce the wide absorption feature at 4057.8Å. Though the assumption of the solar isotope ratio is adequate to derive the Pb abundance, more detailed analysis for this line using a higher quality spectrum

may provide some information on the isotope ratios and give constraints on Pb production.

The lower panel of Figure 6 shows the newly detected Pb I line at 3683.5Å. Though the quality of the spectrum at this wavelength is poorer than at 4057Å, the analysis is easier because blending is not severe; this line is clearly seen even in the solar spectrum. We note that the broad absorption in the shorter wavelength region is the wing of the hydrogen line (H20) at 3682.8Å. The abundance derived from this line ($\log\epsilon(\text{Pb}) = +1.9$) agrees well with that from the $\lambda 4057.8$ line, confirming the Pb abundance derived by the previous works. The effect of isotope shifts and hyperfine splitting was also included in this analysis, but the effect is less remarkable for this line, as shown in the figure.

3.2.2. Dy, Er and Yb

Dysprosium (Dy, $Z = 66$) and Erbium (Er, $Z = 68$) have already been detected by [Aoki et al. \(2001\)](#) ([Aoki et al. \(2001\)](#)) in LP 625-44, but the number of lines studied was quite limited. In our HDS spectrum, several new lines have been discovered in the wavelength range 3600-3700 Å. We analyzed these lines using the transition probabilities taken from [Kusz \(1992\)](#) ([Kusz \(1992\)](#)) and [Musiol et al. \(1983\)](#) ([Musiol et al. \(1983\)](#)) for Dy II and Er II, respectively.

In our new spectrum of LP 625-44, the Ytterbium (Yb, $Z = 70$) II $\lambda 3694.2$ line has been detected. We tried to derive the abundance by spectrum synthesis adopting the line data used in [Snedden et al. \(1996\)](#) ([Snedden et al. \(1996\)](#)). Since there is no useful data on hyperfine splitting, at least to our knowledge, the effect was not included in the analysis. This may cause a significant overestimate of the abundance, because this element has seven stable isotopes, and two of them (^{171}Yb and ^{173}Yb) have odd neutron number. The Yb abundance derived above by single line approximation is much higher than those of Er ($Z = 68$) and Hf ($Z = 72$), but we suspect this is not real and due to the effect of the line splitting.

3.3. Light elements

3.3.1. Carbon and nitrogen

The carbon abundance of LP 625-44 was derived from the CH ($\lambda 4323$) band by [Aoki et al. \(2001\)](#) ([Aoki et al. \(2001\)](#)). We first applied these analyses to our two objects. The carbon abundance ratio derived from the CH band is $[\text{C}/\text{Fe}]=0.27$ and $[\text{C}/\text{Fe}]=2.17$ for HD 140283 and LP 625-44, respectively. In addition to the CH band, the C_2 Swan bands also appear in the spectrum of LP 625-44. Figure 7 shows three bands of the Swan system of this object and the synthetic spectra fitted to the observed one. The derived abundances are $[\text{C}/\text{Fe}]=2.37$, 2.37 and 2.47 for 1-0, 0-0 and 0-1 bands of the system, respectively. These abundances are systematically higher than that derived from the CH band, but the agreement is acceptable giving the uncertainty of the oscillator strengths of these molecular

lines. We adopted carbon abundance $[C/Fe]=2.25$ for LP 625-44.

The absorption lines of neutral carbon around 7110 \AA have also been detected in LP 625-44. We performed the standard analysis for these lines assuming LTE, and derived $[C/Fe]=2.7$. However, the abundance determined from these lines may not be reliable, because the excitation potentials of these lines are quite high ($\sim 8.6 \text{ eV}$), and the resulting abundance is quite sensitive to the model atmosphere and adopted effective temperature. [Tomkin et al. \(1992\)](#) ([Tomkin et al. \(1992\)](#)) studied carbon abundances for halo dwarfs based on C I lines at 9100 \AA , which are also high excitation (7.48 eV) lines like those at 7100 \AA , and found that the carbon abundances derived from the C I lines are considerably higher ($\sim 0.4 \text{ dex}$) than those from CH molecular lines. In their study the non-LTE effect on the abundance determination was investigated for the C I lines, but that is not significant ($< 0.1 \text{ dex}$) for objects with $T_{\text{eff}} \lesssim 5500 \text{ K}$. Our result indicates a similar discrepancy between the carbon abundances derived from C I lines and those from the CH molecular band. [Tomkin et al. \(1992\)](#) ([Tomkin et al. \(1992\)](#)) also found a correlation between carbon abundances from the C I lines and effective temperatures, while there is no temperature dependence for carbon abundances based on CH lines. They pointed out possible inadequacies in the non-LTE analysis and/or model atmosphere used in the analysis for C I lines. Considering these problems in abundance analysis using high excitation C I lines, we adopted the carbon abundances derived from molecular lines as mentioned above.

In the spectrum of LP 625-44, the absorption band of CN violet system ($\lambda 3883$) was also detected. Following [Aoki et al. \(2001\)](#) ([Aoki et al. \(2001\)](#)) we determined the nitrogen abundance ($[N/Fe]=0.95$) from this band. However, it should be noted that the uncertainty in nitrogen abundance derived from CN bands is large, as discussed in [Aoki et al. \(2001\)](#) ([Aoki et al. \(2001\)](#)) in detail.

3.3.2. Oxygen

The oxygen triplet around 7770 \AA has also been detected in both objects. The observed spectra at this wavelength are shown in Figure 8 (dots). The standard analysis was performed for these lines. The derived abundances are $[O/Fe]=+0.91$ and $+1.85$ for HD 140283 and LP 625-44, respectively. We note that the absorption features of $\lambda 7775.4$ in HD 140283 and $\lambda 7772.0$ in LP 625-44 seem to be affected by some noise, like a cosmic-ray event or fringes, and these lines are excluded in the standard analysis. In the figure, synthetic spectra calculated for the derived oxygen abundances and those changed by $\Delta[O/Fe]=\pm 0.3 \text{ dex}$ are shown (lines).

The oxygen abundances in metal-poor dwarfs and subgiants are now in controversy. The abundances derived from these triplet lines are usually higher than those from the $\lambda 6300$ and $\lambda 6363$ forbidden lines in metal-poor dwarfs and subgiants (e.g., [McWilliam 1997](#)). For instance, the oxygen abundance of HD 140283 derived in this analysis ($[O/Fe]=+0.91$) is consistent with the expected value for $[Fe/H] \sim -2.5$ from the trend of oxygen abundances derived from the

triplet lines (e.g., [Boesgaard et al. \(1999\)](#)). However, our oxygen abundance is higher by about 0.5 dex than the one expected from [OI] lines. In fact, though the [O I] lines have not been detected in our objects, the upper limits on the oxygen abundances estimated from the [O I] λ 6300 line (3σ level of equivalent widths evaluated from the S/N ratios at the wavelength) are $[O/Fe]=0.76$ and 1.35 for HD 140283 and LP 625-44, respectively, lower than the oxygen abundances determined by the O I triplet lines.

The discrepancy between the oxygen abundances derived from the O I triplet and those from [O I] lines is beyond the scope of this paper. The important result here is that the oxygen abundance of LP 625-44 is obviously much higher (perhaps by nearly 1.0 dex) than that of HD 140283.

3.3.3. Sodium

Figure 9 shows the observed spectra around the Na I lines. The Na I D lines in LP 625-44 are clearly stronger than those of HD 140283 (lower panel), and the doublet lines with higher excitation around 5685\AA , which do not appear in HD 140283, are detected in LP 625-44. This fact indicates a large excess of Na in LP 625-44. The standard analysis for Na lines derived $[Na/Fe]=+1.75$ for LP 625-44 and $[Na/Fe]=+0.01$ for HD 140283. The Na abundance of LP 625-44 is based on five weak lines as well as strong D lines, implying the result is quite reliable. This remarkable overabundance of Na in LP 625-44 will give a new constraint on the study of the process which produces the abundance pattern of this carbon-rich object (see section 4.2).

3.4. Uncertainties

The internal errors in the abundance determination were estimated by the scatter (standard error) of the abundances derived from individual lines. When the number of lines used in the abundance analysis is too small, we assumed the random error to be 0.2 dex, which is almost the largest scatter in the above analysis. The errors in the abundance determination from the uncertainties of the atmospheric parameters were evaluated by adding in quadrature the individual errors corresponding to $\Delta T_{\text{eff}} = 100\text{K}$, $\Delta \log g = 0.3$, and $\Delta v = 0.5\text{km s}^{-1}$. The uncertainties estimated for the ΔT_{eff} and $\Delta \log g$ are usually 0.05-0.10 dex. The uncertainty due to that of micro-turbulence is strongly dependent on the strength of the lines used in the analysis, and sometimes as large as 0.15-0.2 dex (e.g., for Al, Ni). The uncertainties estimated are given in Table 4 for the abundance ratio ($[X/Fe]$), except for iron for which the uncertainty of $[Fe/H]$ is given. We have discussed the difficulty of the abundance determination for O and Yb. Since the uncertainties of the abundances for these elements cannot be estimated by the above procedure, those are not given in the table.

3.5. Comparison with previous works

The abundances of HD 140283 determined by the present study generally agree very well with those by [Ryan, Norris & Beers \(1996\)](#) ([Ryan, Norris & Beers \(1996\)](#)). The difference of the $[\text{Fe}/\text{H}]$ is 0.02 dex, and those of $[\text{X}/\text{Fe}]$ are less than 0.2 dex. An exception is Yttrium (Y), for which we derived the abundance lower by 0.9 dex than that of [Ryan, Norris & Beers \(1996\)](#) ([Ryan, Norris & Beers \(1996\)](#)), but they commented that their abundance of Y for this object was questionable.

The carbon abundance of HD 140283 was determined by [Ryan, Norris & Bessell \(1991\)](#) ([Ryan, Norris & Bessell \(1991\)](#)). The carbon abundance determined by our analysis ($[\text{C}/\text{Fe}]=0.27$) is consistent with their result ($[\text{C}/\text{Fe}]=0.4$) within the uncertainty. The oxygen abundance of HD 140283 was studied by [Boesgaard et al. \(1999\)](#) ([Boesgaard et al. \(1999\)](#)). Their result derived from the O I triplet lines adopting $T_{\text{eff}}=5694$ K, which is similar to ours, is $[\text{O}/\text{Fe}]=+0.86$, and the agreement is fairly good.

There is no systematic difference between the abundances of neutron capture elements derived here and those by [Aoki et al. \(2001\)](#) ([Aoki et al. \(2001\)](#)) for LP 625-44. The discrepancies are rather large (0.3-0.4 dex) in Dy, Er and Hf. The numbers of lines studied by [Aoki et al. \(2001\)](#) ([Aoki et al. \(2001\)](#)) for these elements were quite limited. We expect the present study improves the abundance determination for these elements by increasing the number of lines used in the analysis. The carbon and nitrogen abundances derived here for LP 625-44 agree with those by [Aoki et al. \(2001\)](#) ([Aoki et al. \(2001\)](#)) within the uncertainties.

For other elements of LP 625-44, we found generally good agreement between the abundances derived here and those by [Norris, Ryan & Beers \(1997\)](#) ([Norris, Ryan & Beers \(1997\)](#)). Exceptions are Sc and Ni, for which [Norris, Ryan & Beers \(1997\)](#) ([Norris, Ryan & Beers \(1997\)](#)) derived by 0.8-0.9 dex higher abundances than ours. They used only one Sc II line and two Ni I lines in their analysis. We have not used these lines because the lines are not covered by our spectra or seem to be affected by blending. Instead we used other 3 Sc lines and 9 Ni lines which are clearly detected in the bluer ($\lambda < 3600\text{\AA}$) region of our spectra. We suspect that the previous results were affected by blending, and believe our new result is more reliable than that by the previous work.

4. Discussion

4.1. Overall abundance patterns

Figure 10 shows the results of abundance analysis for HD140283 (open boxes) and LP 625-44 (filled circles). These two subgiants are known to have quite similar stellar parameters

to each other. Since HD 140283 is a "normal" metal-poor subgiant which represents the typical abundance pattern shared by the other metal-poor subgiants, it is of great interest to compare the abundance pattern of LP 625-44 with that of HD 140283 in order to identify several specific characteristics of this object.

A glance at this figure tells us that the abundance ratios $[X/Fe]$ in LP 625-44 are generally higher than those in HD 140283, except for the elements which have $20 \leq Z \leq 28$. Large enhancement of carbon, nitrogen, and neutron-capture elements has already been studied in detail (Norris, Ryan, & Beers 1997; Aoki et al. 2001). The present study has confirmed several findings in the previous analyses. In addition, we found for the first time a remarkable excess of O, Na, Mg, and Al in LP 625-44. We will discuss characteristics of these light elements below.

The abundance patterns of elements with $20 \leq Z \leq 28$ in LP 625-44 and HD 140283 are very similar to each other, and are typical of metal-poor stars in the same metallicity range. Compared with the solar system abundance ratios, Ca and Ti are moderately overabundant by ~ 0.3 dex, and Cr and Mn are rather underabundant by $0.2 \sim 0.5$ dex, while Co is overabundant by ~ 0.2 dex.

4.2. Oxygen and sodium overabundances

Goriely & Mowlavi (2000) have recently carried out a parametric study of the *s*-process nucleosynthesis including the production of the light elements. Their model adopts one parameter of partial mixing of protons from the hydrogen-rich envelope into the carbon-rich layers during the third dredge-up. Protons which are supplied into the carbon-rich layer produce ^{13}C , which is the major neutron source through the $^{13}\text{C}(\alpha, n)^{16}\text{O}$ process for subsequent *s*-process nucleosynthesis in their model. They studied the efficiency of producing the light elements and the *s*-process elements by adopting various proton abundances in the partial mixing zone.

When the proton mixing is extremely strong ($X_p^{mix} > 10^{-2}$ in their model), hydrogen burning occurs in the ^{12}C -rich and ^{22}Ne -rich layer, and produces large overabundances of ^{14}N and ^{23}Na as shown in Figure 1 in Goriely & Mowlavi (2000). The expected process for the production of enriched ^{23}Na in LP 625-44 is the proton capture by ^{22}Ne , i.e. $^{22}\text{Ne}(p, \gamma)^{23}\text{Na}$. However, if this is the case, the hydrogen burning does not produce ^{13}C efficiently in order to provide enough free neutrons for the *s*-process. This leads to a difficulty in finding strongly enhanced *s*-process elements in this star as shown in Figure 10.

The moderately proton-rich case ($X_p^{mix} \sim 10^{-2}$) is likely to explain large ^{13}C excess, which can provide enough neutrons for the *s*-process nucleosynthesis, at the risk of losing ^{23}Na because the proton capture by ^{22}Ne does not occur efficiently. Moderate enhancement in ^{16}O and ^{24}Mg are expected, which is in reasonable agreement with the abundances derived from our analysis of LP 625-44.

Having these discussions, we are now forced to speculate that the abundance pattern of LP 625-44 may be explained in the hybrid model which exhibits both a high proton-density

zone and a moderate proton-density zone. Physical processes which induce the proton mixing are still unknown, although diffusion effects and stellar rotation are possible candidates (Goriely & Mowlavi 2000, and references therein). Our result gives a new, strong constraint on such types of proton mixing models of the AGB evolution.

It is worthwhile studying another scenario of the s -process nucleosynthesis in AGB stars which has recently been proposed by Iwamoto et al. (2001), that is a model which enables the proton mixing into the helium burning layers at thermal pulses (see the next subsection).

4.3. Ratio between abundances of elements at second and third s -process peaks

Detection of Pb I λ 3683 in the present work has confirmed the accuracy of the previously determined Pb abundance $[\text{Pb}/\text{Fe}] = 2.6$ (Aoki et al. 2000; Aoki et al. 2001). Pb is a unique, accessible element among those at the third abundance peak, while there are several elements, Sr-Y-Zr at the first abundance peak and Ba-to-Nd at the second abundance peak, which previously been detected in several metal-deficient stars. We discuss in this subsection the ratios of the abundances of the second-peak elements to the abundance of Pb, which have shown a large difference among several recently observed s -process-element-rich stars.

We here define an average abundance ratio of elements in the second s -process peak to those in the third s -process peak by $[\text{hs}/\text{Pb}] = ([\text{La}/\text{Fe}] + [\text{Ce}/\text{Fe}] + [\text{Nd}/\text{Fe}])/3 - [\text{Pb}/\text{Fe}]$, where 'hs' means 'heavy' s -process elements as used in some previous papers. This ratio turns out to be $[\text{hs}/\text{Pb}] = -0.36$ for LP 625-44 (this work), and -0.41 for LP 706-7 (Norris, Ryan & Beers 1997; Aoki et al. 2000). These values are similar to each other. Recently, van Eck et al. (2001) have studied another three s -process-element-rich stars HD187861 ($[\text{Fe}/\text{H}] = -1.65$), HD224959 ($[\text{Fe}/\text{H}] = -1.7$), and HD196944 ($[\text{Fe}/\text{H}] = -2.45$) which exhibit considerably smaller abundance ratios $[\text{hs}/\text{Pb}] = -1.14$, -1.13 , and -1.23 , respectively. We plot the $[\text{hs}/\text{Pb}]$ values as a function of metallicity $[\text{Fe}/\text{H}]$ for all these five stars in Figure 11.

Although the sample of metal-poor, s -process element-rich stars is still too small to infer some definite conclusion, one speculative possibility is that a different nucleosynthesis condition might produce a large scatter in the abundance ratios of s -process elements. The s -process in low metallicity AGB stars has ever been studied theoretically by Gallino et al. (1998) and Goriely & Mowlavi (2000), based on the scenario of s -process in the radiative layer between two thermal pulses. In these theoretical models they introduced one adjustable parameter to treat the proton supply to the ^{12}C -rich layer where ^{13}C is produced as the major neutron source for the s -process. Since the neutron exposure in the s -process in AGB stars depends strongly on this parameter, a large scatter in $[\text{hs}/\text{Pb}]$ may result from different conditions of the adopted parameter values although the mechanism of proton mixing is unknown in their models.

Another possibility arises from the speculation that there are at least two types of nucleosynthesis processes to give rise to different abundance ratios $[\text{hs}/\text{Pb}] \approx -0.4$ (for LP 625-44 and LP 706-7) and -1.2 (for HD187861, HD224959, and HD196944). Quite recently,

te]cite.iwamoto02Iwamoto et al. (2002) ([cite]cite.iwamoto02Iwamoto et al. (2002)) have found theoretically that the proton mixing into helium burning layer occurs at thermal pulses only in very metal-deficient ($[\text{Fe}/\text{H}] \leq -2.5$) AGB stars. This kind of mixing is prevented by the large entropy barrier between the helium-rich zone and the hydrogen-rich envelope in the stars with higher metallicity (000 [cite]cite.fujimoto00Fujimoto, Ikeda & Iben(2000)). They have also shown that the *s*-process proceeds under a condition of large neutron exposure in the convective helium burning shell so that the resultant *s*-process abundance pattern fits very well to that observed in two metal-deficient stars LP 625-44 and LP 706-7 but is different from those in the three stars studied by te]cite.vaneck01van Eck et al. (2001) ([cite]cite.vaneck01van Eck et al. (2001)). This theoretical prediction should be tested by further observation of the metallicity dependence of $[\text{hs}/\text{Pb}]$ in the *s*-process element-rich stars.

Further studies of the *s*-process nucleosynthesis in metal-deficient AGB stars are desired to correctly interpret the difference in $[\text{hs}/\text{Pb}]$ found in the present study. It is also important to study the origin of Pb in the solar system, which is one of the long-standing problems in the chemical evolution of the Galaxy, by clarifying the difference from the *s*-process nucleosynthesis in the metal-deficient AGB stars. Note, however, that any theoretical models are required to explain not only the abundance ratios of neutron-capture elements but also several characteristics of the light elements which were discussed in the previous subsection.

5. Concluding remarks

The high resolution spectrum with wide wavelength coverage obtained with Subaru/HDS for the carbon-rich, very metal-poor star LP 625-44 provided new constraints on the modelings for the *s*-process at low metallicity and AGB evolution. We found significant overabundances in some light elements, in addition to carbon and nitrogen whose enhancement has already been known. The Na enhancement in LP 625-44 is significant, suggesting that hydrogen burning in the ^{22}Ne -rich layer in an AGB star produces the abundance pattern of this object. The oxygen abundance was derived from O I triplet around 7770\AA , and the excess of oxygen in LP 625-44 is also remarkable (\sim factor 10) compared with that of HD 140283, though there are uncertainties in the oxygen abundances which are well known in metal-poor dwarfs and subgiants. The newly detected Pb I $\lambda 3683\text{\AA}$ line confirmed the Pb abundance derived by the previous work from the Pb I $\lambda 4057\text{\AA}$ line. The abundance ratio of the elements at the second peak to the third peak of the *s*-process ($[\text{hs}/\text{Pb}]$ defined in the present work) shows a large spread (or two distinct classes) in the *s*-process element-rich stars. Further study for a much larger sample covering a wide metallicity range is crucial to investigate the characteristics of the *s*-process in the early Galaxy.

The next step of the study on the *s*-process element-rich stars like LP 625-44 is the measurements of the neutron densities and temperatures during the *s*-process. These parameters will distinguish the processes occurring during the thermal pulse (short time-scale processes

with high neutron density and high temperature) and those occurring during the inter-pulse phase (long time-scale processes with low neutron density and low temperature). The estimation of neutron density and temperature for the processes which have contributed to the abundances of the observing object may be possible by the measurements of isotope ratios for some elements near the branching points (e.g., ^{151}Sm). The high resolving power of HDS will provide an opportunity for isotope studies of these objects.

We are grateful to N. Iwamoto for fruitful discussions on this topic. Thanks are due to S.G. Ryan for reading the manuscript with helpful comments.

References

- [Aoki et al.(2000)] Aoki, W., Norris, J. E., Ryan, S. G., Beers, T. C., Ando, H. 2000, *ApJ*, 536, L97
- [Aoki et al. (2001)] Aoki, W., Ryan, S.G., Norris, J.E., Beers, T.C., Ando, H., Iwamoto, N., Kajino, T., Mathews, G. J. & Fujimoto, M.Y., 2001, *ApJ*, 561, 346
- [Bard, Kock & Kock (1991)] Bard, A., Kock, A. & Kock, M., 1991, *A&A*, 248, 315
- [Bergström et al. (1988)] Bergström, H., Biémont, E., Lundberg, H. & Persson, A., 1988, *A&A*, 192, 335
- [Biémont et al. (1989a)] Biémont, E., Grevesse, N., Faires, L.M., Marsden, G., Lawler, J.E. & Whaling, W., *A&A*, 1989a, 209, 391
- [Biémont et al. (1989b)] Biémont, E., Grevesse, N., Hannaford, P. & Lowe, R. M., 1989b, *A&A*, 222, 307
- [Bizzarri et al. (1993)] Bizzarri, A., Huber, M. C. E., Noels, A., Grevesse, N., Bergeson, S. D., Tsekeris, P. & Lawler, J. E., 1993, *A&A*, 273, 707
- [Blackwell et al. (1989)] Blackwell, D. E., Booth, A. J., Petford, A. D. & Laming, J. M., 1989, *MNRAS*, 236, 235
- [Boesgaard et al. (1999)] Boesgaard, A.M., King, J.R., Deliyannis, C.P. & Vogt, S.S., 1999, *AJ*, 117, 492
- [Bord, Barisciano & Cowley (1996)] Bord, D. J., Barisciano, L. P. & Cowley, C. R., 1996, *MNRAS*, 278, 997
- [Corliss & Bozman (1962)] Corliss, C. H. & Bozman, W. R., 1962, *Experimental Transition Probabilities for Spectral lines of Seventy Elements* (NBS Monograph 53; Washington: GPO)
- [Cowley & Corliss (1983)] Cowley, C. R. & Corliss, C. H., 1983, *MNRAS*, 203, 651
- [Fujimoto, Ikeda & Iben(2000)] Fujimoto, M. Y., Ikeda, Y. & Iben, I. Jr, 2000, *ApJ*, 529, L25
- [Fuhr, Martin & Wiese (1988)] Fuhr, J.R., Martin, G.A. & Wiese, W.L., 1988, *J. Phys. Chem. Ref. Data*, 17, suppl. 4
- [Fuhrmann (1998)] Fuhrmann, K., 1998, *A&A*, 330, 626
- [Gallino et al. (1998)] Gallino, R., Arlandini, C., Busso, M., Lugaro, M., Travaglio, C., Straniero, O., Chieffi, A. & Limongi, M., 1998, *ApJ*, 497, 388
- [Gigas (1988)] Gigas, D., 1988, *A&A*, 192, 264

- [Goly et al. (1991)] Goly, A., Kusz, J., Nguyen Quang, B. & Weniger, S., 1991, *J. Quant. Spectrosc. Radiat. Transfer*, 45, 157
- [Goriely & Mowlavi (2000)] Goriely, S. & Mowlavi, N., 2000, *A&A*, 362, 599
- [Grevesse et al. (1981)] Grevesse, N., Biéumont, E., Lowe, R.M. & Hannaford, P., "Chemically peculiar stars of the upper main sequence" 23rd International Conference on Astrophysics, 211
- [Hannaford et al. (1982)] Hannaford, P., Lowe, R. M., Grevesse, N., Biéumont, E. & Whaling, W., 1982, *ApJ*, 261, 736
- [Heise & Kock (1990)] Heise, C. & Kock, M., 1990, *A&A*, 230, 244
- [Hirata & Horaguchi (1994)] Hirata, R. & Horaguchi, T., 1994, <ftp://cdsarc.u-strasbg.fr/cats/VI/69/>
- [Iben & Renzini (1983)] Iben, I. Jr. & Renzini, A., 1983, *ARA&A*, 21, 271
- [Iwamoto et al. (2002)] Iwamoto, N., Kajino, T., Mathews, G. J., Fujimoto, M. Y. & Aoki, W., 2001, *J. Nucl. Sci. and Tech.*, in press
- [Jönsson et al. (1984)] Jönsson, G., Kröll, S., Persson, A. & Svanberg, S., 1984, *Phys.Rev. A*30, 2429
- [Kastberg et al. (1993)] Kastberg, A., Villemoes, P., Arnesen, A., Heijkenskjöld, F., Langereis, A., Jungner, P. & Linnæus, S., 1993, *J.Opt.Soc.Amer.*, B10, 1330
- [King et al. (1998)] King, J.R., Stephens, A., Boesgaard, A. M. & Deliyannis, C.P., 1998, *AJ*, 115, 666
- [Kurucz (1993)] Kurucz, R. L., 1993, CD-ROM 13, ATLAS9 Stellar Atmospheres Programs and 2km/s Grid (Cambridge: Smithsonian Astrophys. Obs.)
- [Kurucz & Bell (1995)] Kurucz, R. L. & Bell, B., 1995, CD-ROM 23, Atomic Line List (Cambridge: Smithsonian Astrophys. Obs.)
- [Kusz (1992)] Kusz, J., 1992, *A&AS*, 92, 517
- [Lawler & Dakin (1989)] Lawler, J.E. & Dakin, J.T., 1989, *J.Opt.Soc.Amer.* B6, 1457
- [Manning, Anderson & Watson (1950)] Manning, T. E., Anderson, C. E. & Watson, W. W., 1950, *Phys. Rev.*, 78, 417
- [Martin, Fuhr & Wiese (1988)] Martin, G. A., Fuhr, J. R. & Wiese, W. L., 1988, *J. Phys. Chem. Ref. Data*, 17 Suppl. 3
- [Morton (1991)] Morton, D.C., 1991, *ApJS*, 77, 119
- [McWilliam et al. (1995)] McWilliam, A., Preston, G. W., Sneden, C. & Searle, L., 1995, *AJ*, 109, 2757
- [McWilliam (1997)] McWilliam, A., 1997, *ARA&A*, 35, 503
- [Musiol et al. (1983)] Musiol, K. & Labuz, S., 1983, *Phys. Scr.*, 27, 422
- [Norris, Ryan & Beers (1996)] Norris, J. E., Ryan, S. G. & Beers, T. C., 1996, *ApJS*, 107, 391
- [Norris, Ryan & Beers (1997)] Norris, J. E., Ryan, S. G. & Beers, T. C., 1997, *ApJ*, 488, 350
- [O'Brian et al. (1991)] O'Brian, T.R., Wickliffe, M.E., Lawler, J.E., Whaling, W. & Brault, J.W., 1991, *J. Opt. Soc. Am. B*, 8, 1185
- [Pauls, Grevesse & Huber (1990)] Pauls, U., Grevesse, N. & Huber, M.C.E., 1990, *A&A*, 231, 536
- [Ryan (1998)] Ryan, S. G., 1998, *A&A*, 331, 1051
- [Ryan, Norris & Beers (1996)] Ryan, S. G., Norris, J. E. & Beers, 1996, *ApJ*, 471, 254
- [Ryan, Norris & Bessell (1991)] Ryan, S. G., Norris, J. E. & Bessell, M. S., 1991, *AJ*, 102, 303
- [Savanov, Huovelin & Tuominen (1990)] Savanov, I.S., Huovelin, J. & Tuominen, I., 1990, *A&AS*, 86, 531

- [Smith et al. (1987)] Smith, P. L., Huber, M.C.E., Tozzi, G.P., Griesinger, H.E., Cardon, B.L. & Lombardi, G.G., 1987, ApJ, 322, 573
- [Smith & Raggett (1981)] Smith, G. & Raggett, D.J., 1981, J.Phys. B14, 4015
- [Sneden et al. (1996)] Sneden, C., McWilliam, A., Preston, G.W., Cowan, J.J., Burris, D. & Armosky, B.J., 1996, ApJ 467, 819
- [Straniero et al. (1995)] Straniero, O., Gallino, R., Busso, M., Chieffi, A., Raiteri, C. M., Limongi, M. & Salaris, M., 1995, ApJ, 440, L85
- [Tomkin et al. (1992)] Tomkin, J., Lemke, M., Lambert, D. L. & Sneden, C., 1992, AJ, 104, 1568
- [Tomkin et al. (1995)] Tomkin, J., Woolf, V. M., Lambert, D. L. & Lemke, M., 1995, AJ, 109, 2204
- [van Eck et al. (2001)] Van Eck, S., Goriely, S., Jorissen, A. & Plez, B., 2001, Nature, 412, 793
- [Ward et al. (1985)] Ward, L. Vogel, O., Arnesen, A., Hallin, R. & Wännström, A., 1985, Phys. Scripta., 31, 161
- [Wiese & Fuhr (1975)] Wiese, W. L. & Fuhr, J. R., 1975, J. Phys. Chem. Ref. Data, 4, 263
- [Wiese & Martin (1980)] Wiese, W. L. & Martin, G. A., 1980, Wavelengths and Transition Probabilities for Atoms and Atomic Ions (NSRDS-NBS No. 68, Part II; Washington: GPO)
- [Youssef & Khalil (1989)] Youssef, N. H. & Khalil, N. M., 1989, A&A, 208, 271

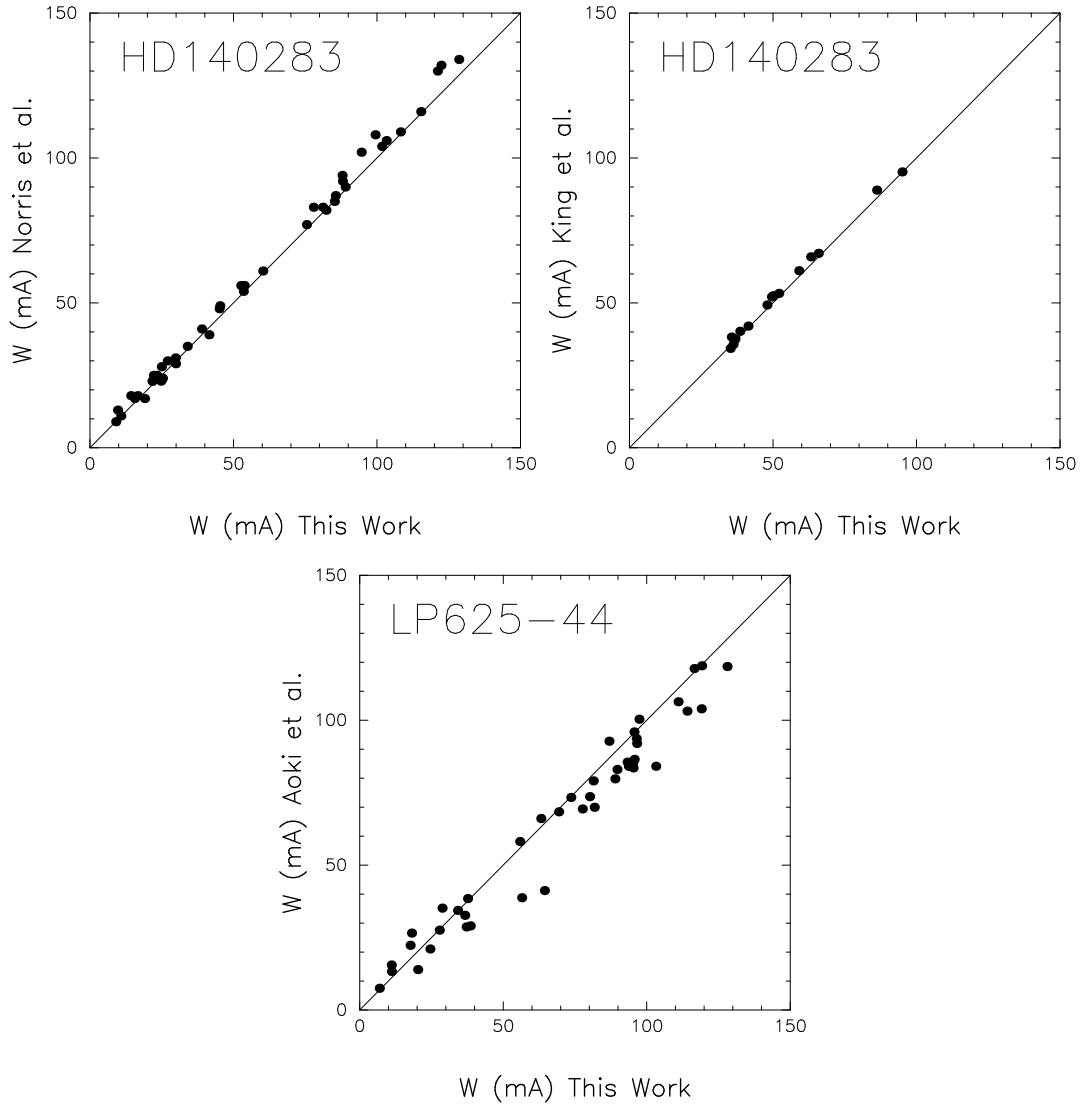


Fig. 1. Comparison of the equivalent widths for Fe I lines measured by the present analysis with those of [Norris, Ryan & Beers \(1996\)](#) ([Norris, Ryan & Beers \(1996\)](#)) and [King et al. \(1998\)](#) ([King et al. \(1998\)](#)) for HD140283 and those of [Aoki et al. \(2000\)](#) ([Aoki et al. \(2000\)](#)) for LP625-44.

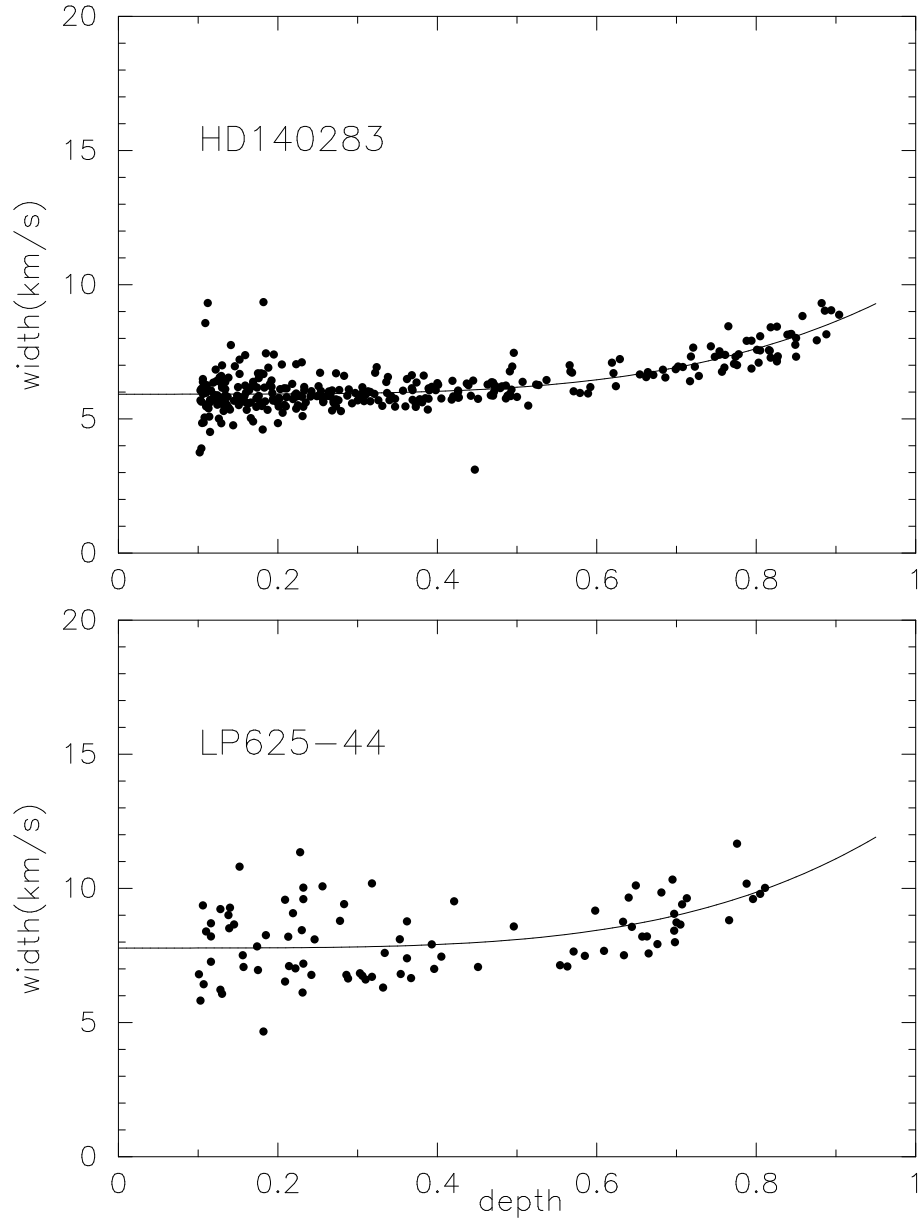


Fig. 2. Line width as a function of depth for Fe I lines for HD 140283 (upper) and LP 625-44 (lower). Here the line width means the Gaussian dispersion in velocity unit (kms^{-1}) corrected for instrumental effect for which we assumed the 3.5kms^{-1} (FWHM) Gaussian profile.

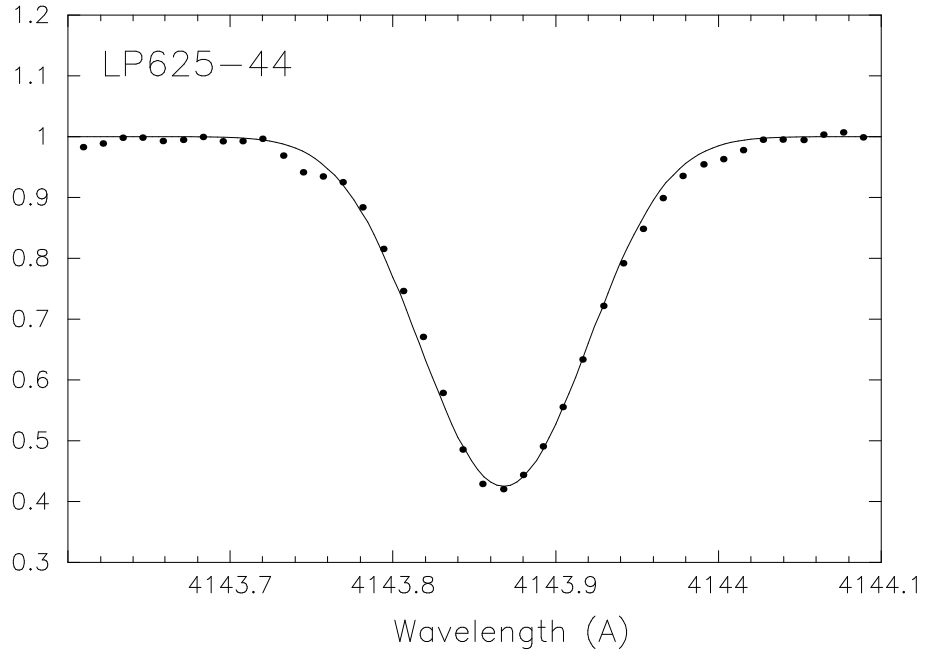


Fig. 3. Observed spectrum of LP 625-44 around the Fe I $\lambda 4143.8$ line (dots). The synthetic spectrum (line) fitted to the observed one is calculated for $v_{\text{macro}} = 6.5 \text{ km s}^{-1}$. (see text for details)

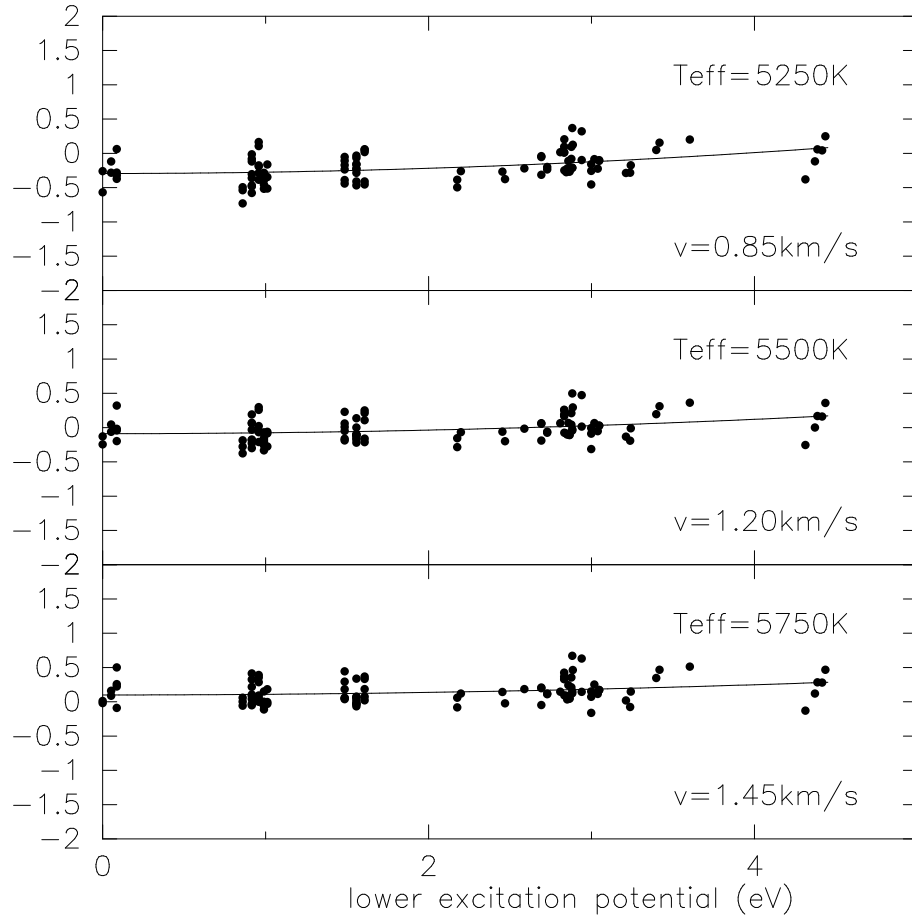
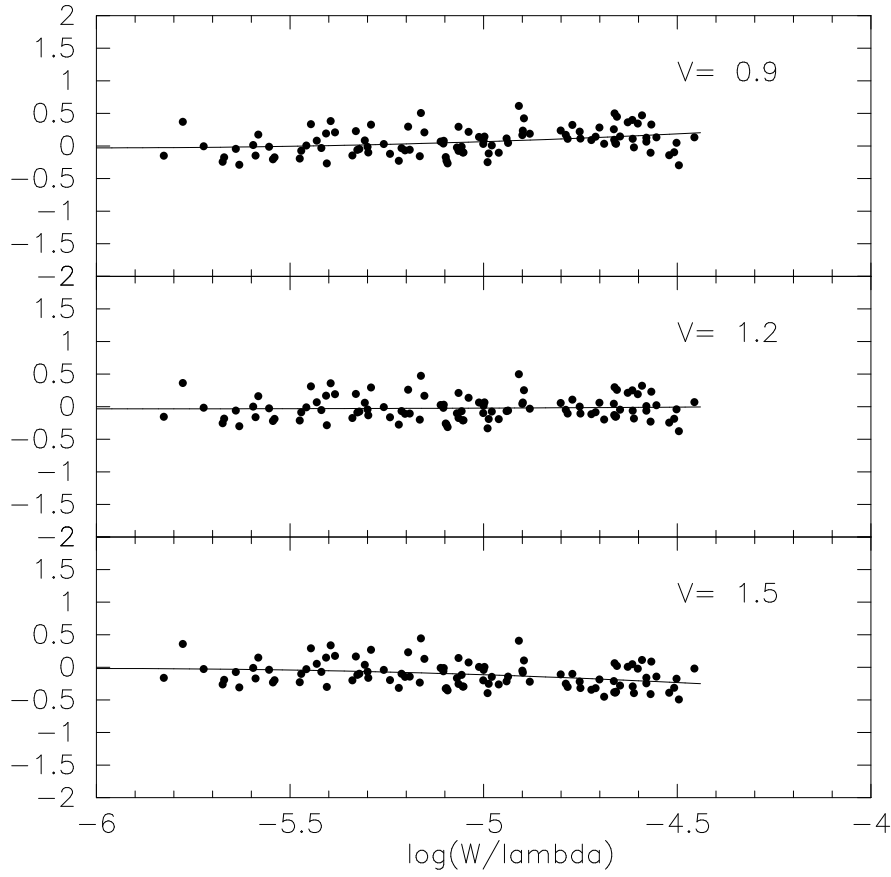


Fig. 4. Logarithmic abundances derived from Fe I lines as a function of the lower excitation potential for LP 625-44. The vertical axis shows the abundance difference from the input (assumed) one in the analysis ($\log \epsilon = 4.8$). The effective temperature assumed and micro-turbulence (v) adopted in the analysis are given in each panel.



waaki 3-Mar-2001 14:23

Fig. 5. Logarithmic abundances derived from Fe I lines as a function of equivalent width of the line for LP 625-44. The micro-turbulent velocity assumed (km s^{-1}) is given in each panel.

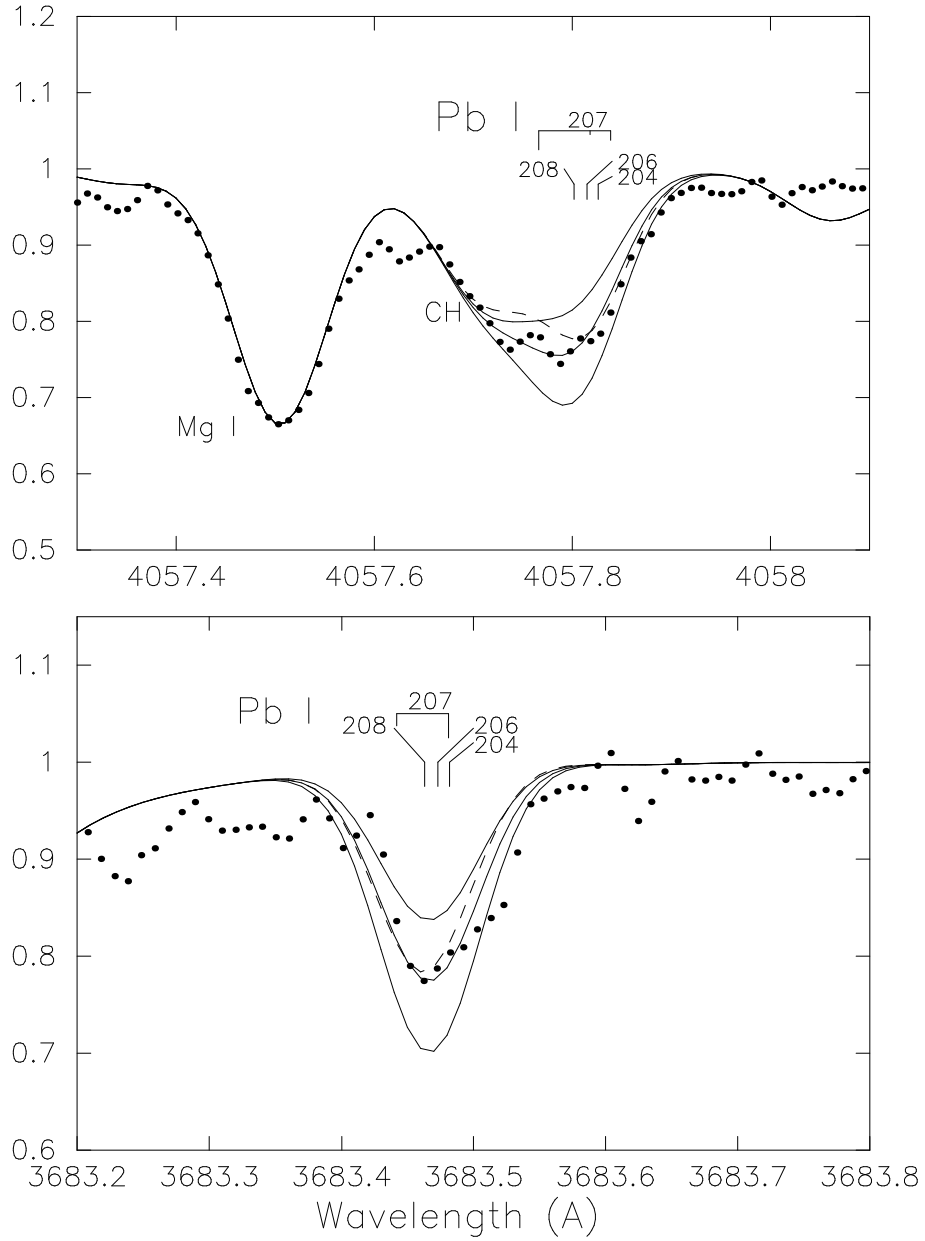


Fig. 6. Observed spectrum of LP 625-44 for Pb I lines at 4057Å (upper) and 3683Å (lower). The synthetic spectra shown by solid lines are calculated including isotope shifts and hyperfine splitting for $[\text{Pb}/\text{Fe}] = +2.6 \pm 0.2$. The line positions of four Pb isotopes are shown in each panel. The dashed lines indicate the synthetic spectra calculated using the single-line approximation.

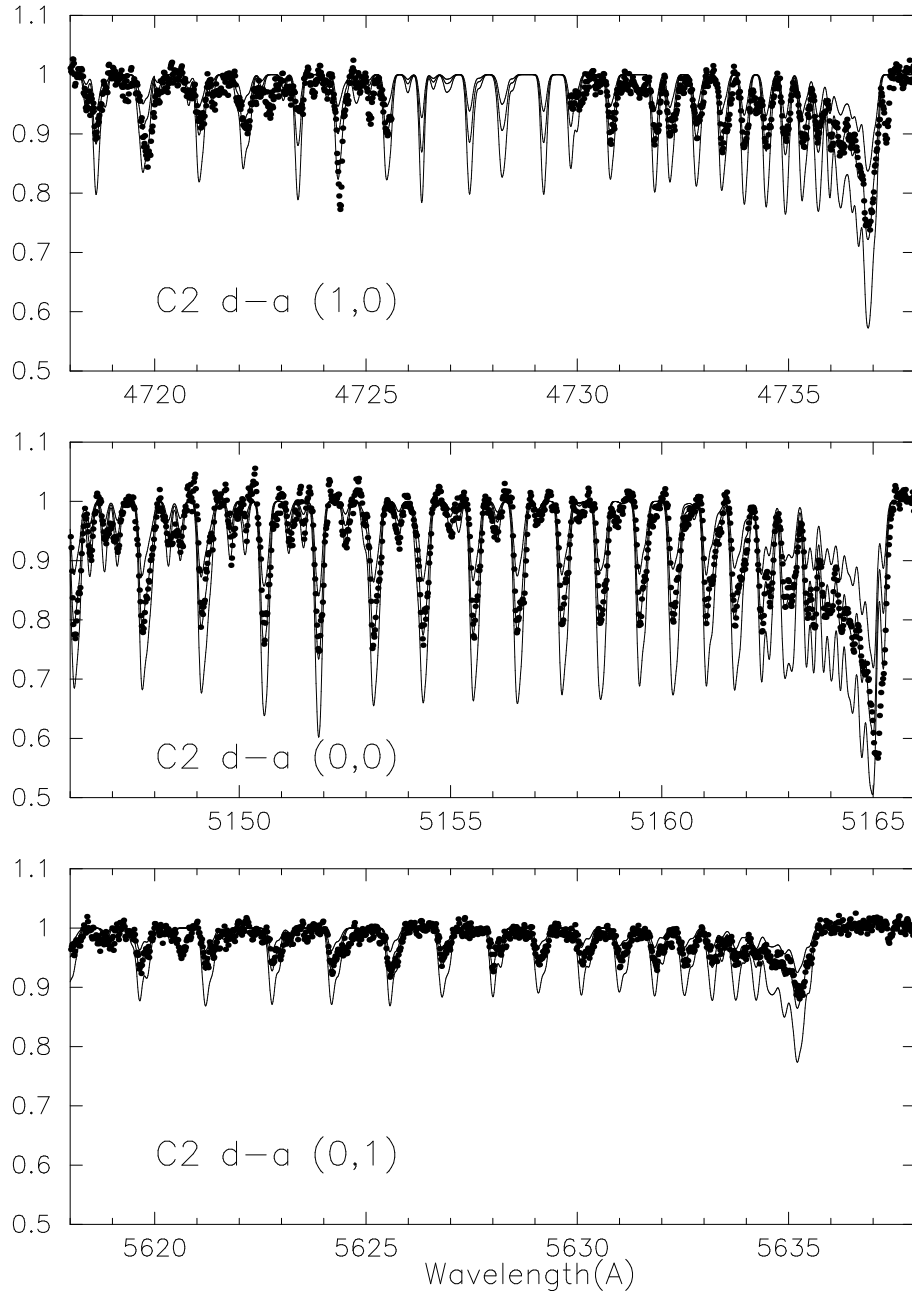


Fig. 7. Observed spectrum of LP 625-44 for three C₂ Swan bands (dots). The central synthetic spectra (lines) are calculated for $[C/Fe]=2.37$, 2.37 and 2.47 for top, middle and bottom panels, respectively. The other spectra are calculated for $\Delta[C/Fe]=\pm 0.15$ difference. The observed spectrum around 4727\AA is excluded because that is affected by a bad column in the detector.

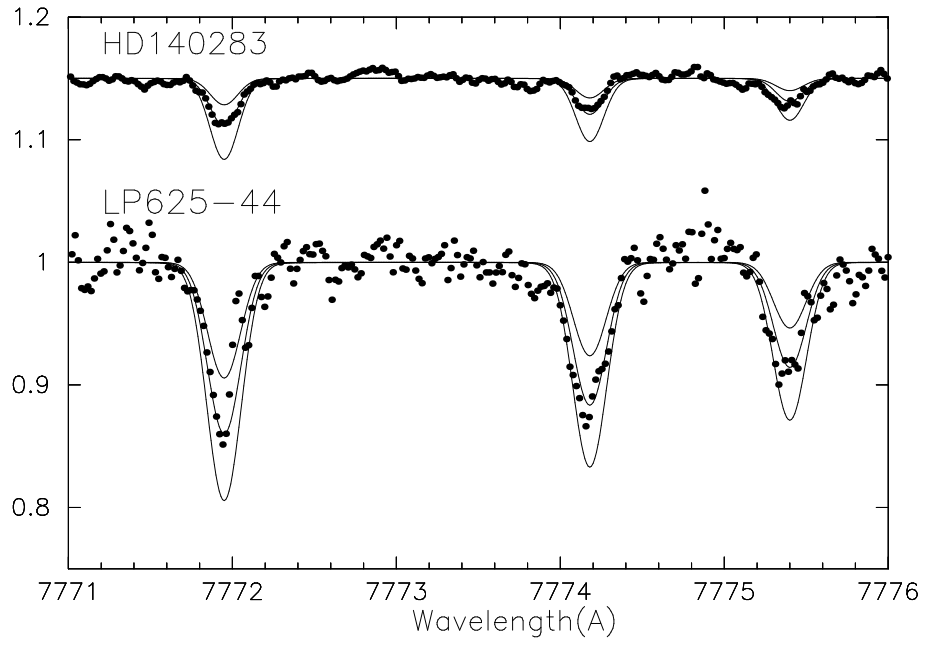


Fig. 8. Observed spectra for O I triplet (dots). The spectrum of HD 140283 is vertically shifted by 0.15. The synthetic spectra (lines) are calculated for $[O/Fe]=0.95\pm 0.3$ and 1.85 ± 0.3 for HD 140283 and LP 625-44, respectively.

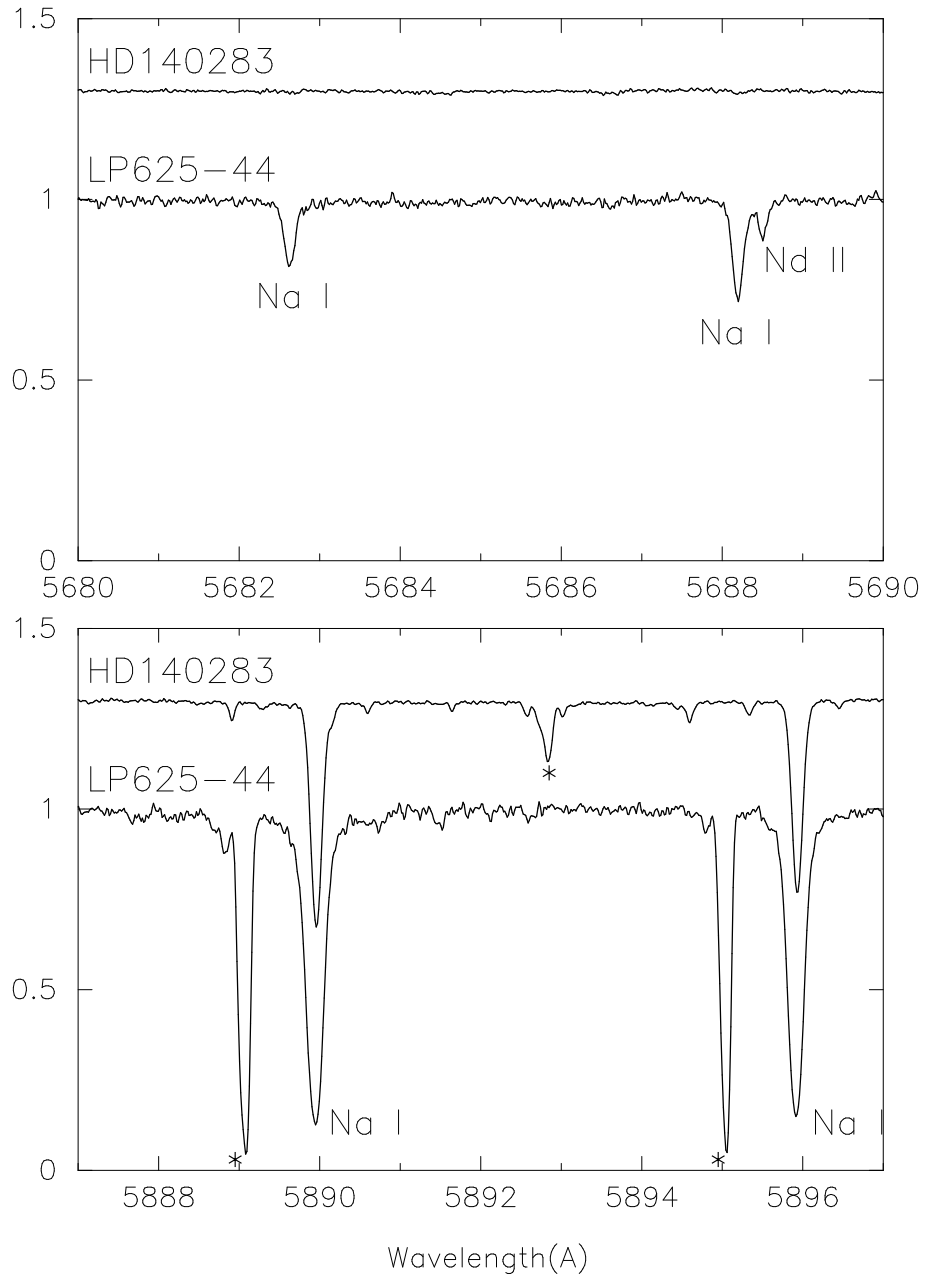


Fig. 9. Observed spectra around Na I lines. The spectrum of HD 140283 is vertically shifted by 0.3. The lines shown by asterisks are those due to interstellar absorption. The Na I lines in LP 625-44 are much stronger than those in HD 140283, indicating a large overabundances of Na in LP 625-44.

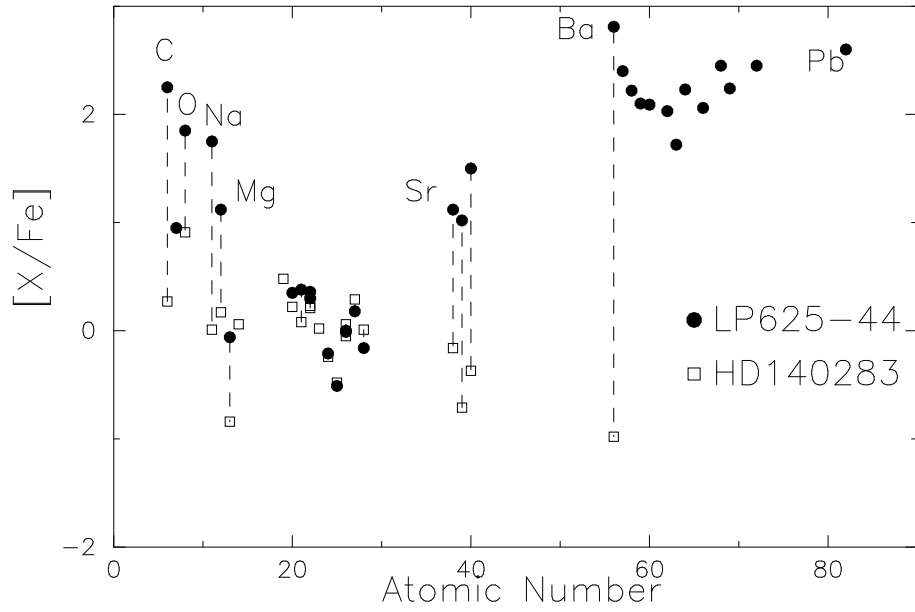


Fig. 10. Abundance ratio ($[X/Fe]$) as a function of atomic number.

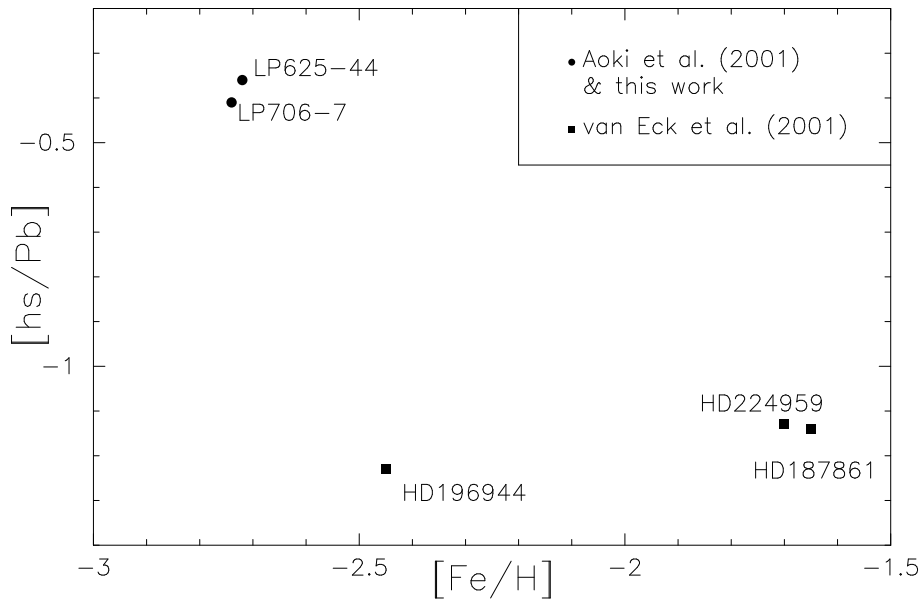


Fig. 11. Ratio between abundances of elements at second and third s -process peaks ($[hs/Pb]$), as a function of $[Fe/H]$ for s -process element-rich stars. The abundance ratio of the second s -process peak is defined as $[hs/Fe] = ([La/Fe] + [Ce/Fe] + [Nd/Fe]) / 3$ (see text for details)

Table 1. Observations

Object	Obs. date	Wavelength(\AA)	exposure (sec)	S/N (Wavelength) ^a
LP 625-44	3 July, 2000	5100-7800	3600	130 (6000 \AA)
	21 Aug, 2000	3400-5100	3600	70 (4000 \AA)
HD 140283	18 Aug, 2000	3100-4500	1800	330 (4000 \AA)
	5 July, 2000	3400-5100	1800	560 (4800 \AA)
	3 July, 2000	5100-7800	960	680 (6000 \AA)

^a S/N ratio per 0.9 km s^{-1} pixel.

Table 2. Radial Velocity Measurement

Object	JD	wavelength Å	Radial velocity (km s ⁻¹)	number of lines
LP 625-44	2451728.9	5100-6500	30.92±0.26	26
	2451777.8	3700-5100	30.20±0.30	46
HD 140283	2451728.8	5100-6500	-170.58±0.15	23
	2451730.9	4500-5100	-170.64±0.34	21

Table 3. Results

Element	Wavelength (Å)	L.E.P. (eV)	$\log gf$	HD140283	LP625-44	
C I	7111.475	8.640	-1.130	...	21.0	(1)
C I	7113.180	8.650	-0.810	...	36.6	(1)
C I	7115.186	8.640	-0.710	...	32.5	(1)
C I	7116.990	8.650	-0.940	...	36.6	(1)
C I	7119.671	8.640	-1.070	...	27.4	(1)
Na I	4978.541	2.102	-1.220	...	12.4	(2)
Na I	4982.813	2.104	-0.960	...	17.2	(2)
Na I	5682.633	2.102	-0.700	...	33.9	(2)
Na I	5688.204	2.104	-0.460	...	51.0	(2)
Na I	5889.951	0.000	0.101	109.5	236.2	(3)
Na I	5895.924	0.000	-0.197	89.4	216.0	(3)
Na I	6154.226	2.102	-1.530	...	4.0	(2)
Mg I	3329.919	2.709	-1.780	37.5	...	(2)
Mg I	3336.674	2.717	-1.100	71.0	...	(2)
Mg I	3829.355	2.709	-0.210	113.5	...	(2)
Mg I	4057.505	4.346	-0.890	...	49.0	(4)
Mg I	4167.271	4.346	-0.770	25.5	...	(4)
Mg I	4702.991	4.346	-0.520	38.3	76.7	(4)
Mg I	5172.685	2.712	-0.380	130.4	161.3	(2)
Mg I	5183.604	2.717	-0.160	142.7	...	(2)
Mg I	5528.404	4.346	-0.490	41.0	75.3	(5)
Al I	3944.006	0.000	-0.644	70.5	...	(3)
Al I	3961.520	0.014	-0.340	69.5	98.5	(2)
Si I	3905.523	1.909	-0.980	114.3	...	(6)
K I	7664.911	0.000	0.135	29.6	...	(3)
K I	7698.974	0.000	-0.168	16.8	...	(3)
Ca I	4226.728	0.000	0.244	122.6	...	(3)
Ca I	4283.010	1.886	-0.220	29.7	...	(2)
Ca I	4289.364	1.879	-0.300	25.0	...	(2)
Ca I	4298.986	1.886	-0.410	28.6	...	(2)
Ca I	4355.079	2.709	-0.420	5.8	...	(2)
Ca I	4425.441	1.879	-0.360	23.1	...	(2)
Ca I	4434.960	1.886	-0.010	37.9	...	(2)
Ca I	4435.688	1.886	-0.520	17.8	...	(2)
Ca I	4454.781	1.899	0.260	48.0	...	(2)

Table 3. (Continued)

Element	Wavelength (Å)	L.E.P. (eV)	$\log gf$	HD140283	LP625-44	
Ca I	4455.887	1.899	-0.530	15.0	...	(2)
Ca I	4526.935	2.709	-0.548	3.8	...	(7)
Ca I	5261.706	2.521	-0.579	5.3	...	(7)
Ca I	5262.244	2.521	-0.471	8.5	...	(7)
Ca I	5349.472	2.709	-0.310	4.9	...	(7)
Ca I	5581.971	2.523	-0.555	4.7	...	(7)
Ca I	5588.757	2.526	0.358	25.9	21.6	(7)
Ca I	5590.120	2.521	-0.571	3.8	...	(7)
Ca I	5594.468	2.523	0.097	18.4	...	(7)
Ca I	5598.487	2.521	-0.087	12.9	16.2	(7)
Ca I	5601.285	2.526	-0.523	5.0	...	(7)
Ca I	5857.452	2.933	0.240	14.8	10.7	(7)
Ca I	6102.722	1.879	-0.770	11.2	...	(7)
Ca I	6122.219	1.886	-0.320	28.9	30.2	(2)
Ca I	6162.172	1.899	-0.090	...	32.8	(2)
Ca I	6717.685	2.709	-0.524	5.1	...	(7)
Ca I	7148.147	2.709	0.137	16.1	...	(7)
Sc II	3353.724	0.315	0.250	51.9	...	(8)
Sc II	3359.678	0.008	-0.738	28.6	...	(3)
Sc II	3361.931	0.000	-0.703	31.8	...	(3)
Sc II	3368.936	0.008	-0.373	42.2	...	(3)
Sc II	3535.713	0.315	-0.460	24.6	...	(8)
Sc II	3567.696	0.000	-0.476	39.9	41.1	(3)
Sc II	3576.340	0.008	0.007	61.8	...	(3)
Sc II	3580.925	0.000	-0.149	59.8	58.9	(3)
Sc II	3590.474	0.022	-0.552	39.1	...	(3)
Sc II	3613.829	0.022	0.417	...	100.3	(3)
Sc II	4246.820	0.315	0.240	66.8	...	(8)
Sc II	4320.745	0.605	-0.250	27.2	...	(8)
Sc II	4324.998	0.595	-0.440	18.0	...	(8)
Sc II	4400.386	0.605	-0.540	18.1	...	(8)
Sc II	4415.544	0.595	-0.670	16.2	...	(8)
Sc II	5031.010	1.357	-0.400	5.1	...	(8)
Sc II	5526.785	1.768	0.020	5.7	...	(8)
Ti I	3314.421	1.067	0.190	7.2	...	(9)
Ti I	3354.633	0.021	0.020	22.4	...	(3)

Table 3. (Continued)

Element	Wavelength (Å)	L.E.P. (eV)	$\log gf$	HD140283	LP625-44
Ti I	3358.271	0.000	-1.190	2.9	... (10)
Ti I	3370.434	0.000	-0.410	7.3	... (10)
Ti I	3371.452	0.048	0.130	23.4	... (3)
Ti I	3377.575	0.021	-0.230	12.3	... (10)
Ti I	3385.941	0.048	-0.220	11.3	... (10)
Ti I	3635.462	0.000	0.103	24.2	20.7 (10)
Ti I	3729.807	0.000	-0.295	16.1	... (10)
Ti I	3741.060	0.021	-0.157	15.2	... (10)
Ti I	3904.784	0.900	0.030	6.7	... (9)
Ti I	3924.526	0.021	-0.881	5.5	... (10)
Ti I	3989.759	0.021	-0.142	20.6	... (10)
Ti I	3998.637	0.048	0.000	26.4	25.9 (10)
Ti I	4008.928	0.021	-1.016	4.9	... (10)
Ti I	4024.572	0.048	-0.925	5.8	... (10)
Ti I	4512.733	0.836	-0.424	2.9	... (10)
Ti I	4518.021	0.826	-0.269	4.8	... (10)
Ti I	4533.239	0.848	0.532	16.1	13.2 (10)
Ti I	4534.775	0.836	0.336	12.0	8.3 (10)
Ti I	4617.268	1.749	0.445	2.7	... (10)
Ti I	4681.908	0.048	-1.015	2.8	... (10)
Ti I	4981.730	0.848	0.560	19.0	24.6 (10)
Ti I	4991.066	0.836	0.436	16.8	... (10)
Ti I	4999.501	0.826	0.306	12.6	... (10)
Ti I	5007.206	0.818	0.168	14.2	14.6 (10)
Ti I	5020.024	0.836	-0.358	4.1	... (10)
Ti I	5035.902	1.460	0.260	3.2	... (9)
Ti I	5036.463	1.443	0.186	1.8	... (10)
Ti I	5064.651	0.048	-0.935	5.6	... (10)
Ti I	5173.740	0.000	-1.062	4.7	... (10)
Ti I	5192.969	0.021	-0.948	6.5	... (10)
Ti I	5210.384	0.048	-0.828	5.5	7.1 (10)
Ti II	3203.427	0.000	-1.810	48.7	... (11)
Ti II	3213.147	0.012	-2.270	27.7	... (11)
Ti II	3218.267	1.572	-0.160	48.7	... (12)
Ti II	3220.467	0.122	-1.870	14.1	... (12)
Ti II	3224.248	1.584	0.040	50.6	... (10)

Table 3. (Continued)

Element	Wavelength (Å)	L.E.P. (eV)	$\log gf$	HD140283	LP625-44
Ti II	3226.774	0.028	-1.790	53.5	... (11)
Ti II	3231.308	0.135	-1.500	59.0	... (10)
Ti II	3232.291	1.116	-0.250	55.5	... (10)
Ti II	3239.656	1.084	-0.230	57.5	... (10)
Ti II	3240.710	0.113	-2.130	11.6	... (12)
Ti II	3260.249	1.161	-1.340	20.8	... (10)
Ti II	3263.692	1.165	-1.110	24.6	... (12)
Ti II	3272.073	1.224	-0.690	49.3	... (10)
Ti II	3275.279	1.080	-1.450	16.1	... (10)
Ti II	3276.767	1.180	-0.820	33.3	... (10)
Ti II	3278.283	1.231	-0.210	50.0	... (10)
Ti II	3278.910	1.084	-0.170	57.8	... (10)
Ti II	3282.323	1.224	-0.290	49.7	... (10)
Ti II	3287.657	1.893	0.340	51.2	... (10)
Ti II	3288.136	0.135	-1.970	36.3	... (11)
Ti II	3288.425	1.243	-1.560	18.8	... (10)
Ti II	3288.581	1.231	-1.350	27.2	... (10)
Ti II	3299.430	0.113	-1.830	17.1	... (11)
Ti II	3302.099	0.151	-2.330	21.3	... (11)
Ti II	3307.720	0.122	-2.630	14.5	... (11)
Ti II	3315.320	1.224	-0.600	41.4	... (10)
Ti II	3319.074	0.135	-2.990	7.3	... (11)
Ti II	3321.697	1.231	-0.320	50.9	... (10)
Ti II	3337.851	1.237	-1.300	18.5	... (10)
Ti II	3352.073	1.221	-1.340	21.0	... (10)
Ti II	3388.766	1.237	-1.030	25.4	... (10)
Ti II	3402.436	1.221	-1.000	33.4	... (10)
Ti II	3407.212	0.049	-2.011	45.0	... (3)
Ti II	3409.821	0.028	-1.890	45.5	... (11)
Ti II	3416.952	1.237	-1.570	10.2	... (10)
Ti II	3443.388	2.048	-1.070	2.4	... (10)
Ti II	3456.400	2.061	-0.230	24.0	... (10)
Ti II	3480.885	1.080	-1.760	7.9	... (12)
Ti II	3489.747	0.135	-1.920	44.0	... (10)
Ti II	3500.344	0.122	-2.020	36.8	32.9 (11)
Ti II	3504.890	1.892	0.180	50.5	... (10)

Table 3. (Continued)

Element	Wavelength (Å)	L.E.P. (eV)	$\log gf$	HD140283	LP625-44
Ti II	3510.862	1.893	0.140	44.5	... (10)
Ti II	3535.408	2.061	-0.210	27.7	... (10)
Ti II	3561.565	0.574	-2.300	15.2	... (10)
Ti II	3565.955	1.165	-1.830	11.1	... (10)
Ti II	3596.043	0.607	-1.220	52.3	... (10)
Ti II	3641.325	1.237	-0.710	48.4	... (10)
Ti II	3741.644	1.582	-0.110	52.8	... (10)
Ti II	3761.882	2.590	-0.610	10.5	... (10)
Ti II	3774.651	0.574	-2.730	8.3	... (10)
Ti II	3776.059	1.582	-1.340	14.1	... (10)
Ti II	3813.394	0.607	-2.020	26.8	... (10)
Ti II	3913.477	1.116	-0.530	67.4	73.8 (10)
Ti II	4012.396	0.574	-1.750	35.0	... (11)
Ti II	4025.120	0.607	-1.980	17.7	... (10)
Ti II	4028.355	1.892	-1.000	13.4	... (10)
Ti II	4053.829	1.893	-1.210	8.8	12.7 (10)
Ti II	4161.527	1.084	-2.160	7.4	... (11)
Ti II	4163.634	2.590	-0.400	14.9	... (10)
Ti II	4184.309	1.080	-2.510	3.7	... (11)
Ti II	4287.875	1.080	-2.020	12.7	... (10)
Ti II	4290.216	1.165	-1.120	48.3	... (10)
Ti II	4300.064	1.180	-0.490	67.5	... (11)
Ti II	4301.923	1.161	-1.200	38.1	... (11)
Ti II	4320.957	1.165	-1.870	10.7	... (10)
Ti II	4330.723	1.180	-2.060	5.1	... (11)
Ti II	4337.876	1.080	-1.130	46.2	... (10)
Ti II	4344.299	1.084	-2.090	9.6	... (10)
Ti II	4350.846	2.061	-1.400	5.9	... (10)
Ti II	4395.004	1.084	-0.510	67.9	... (11)
Ti II	4395.833	1.243	-1.970	7.3	... (11)
Ti II	4399.786	1.237	-1.270	30.7	... (10)
Ti II	4417.715	1.165	-1.430	33.5	... (10)
Ti II	4418.306	1.237	-1.990	8.7	... (11)
Ti II	4441.731	1.180	-2.410	4.7	... (10)
Ti II	4443.775	1.080	-0.700	62.2	62.1 (11)
Ti II	4444.536	1.116	-2.210	5.9	... (11)

Table 3. (Continued)

Element	Wavelength (Å)	L.E.P. (eV)	$\log gf$	HD140283	LP625-44
Ti II	4450.503	1.084	-1.510	23.8	17.1 (11)
Ti II	4464.461	1.161	-2.080	12.0	... (10)
Ti II	4468.517	1.131	-0.600	63.4	69.2 (11)
Ti II	4470.835	1.165	-2.280	5.0	... (10)
Ti II	4488.342	3.124	-0.820	2.5	... (10)
Ti II	4501.269	1.116	-0.760	58.1	56.6 (11)
Ti II	4529.480	1.572	-2.030	6.7	... (10)
Ti II	4533.972	1.237	-0.770	58.0	68.5 (10)
Ti II	4549.612	1.584	-0.450	...	74.8 (10)
Ti II	4563.770	1.221	-0.960	...	56.7 (10)
Ti II	4571.957	1.572	-0.530	...	63.2 (10)
Ti II	4657.212	1.243	-2.320	4.3	... (11)
Ti II	4708.651	1.237	-2.370	3.5	... (11)
Ti II	4779.979	2.048	-1.370	5.2	... (10)
Ti II	4798.507	1.080	-2.670	1.9	... (11)
Ti II	4805.089	2.061	-1.100	10.2	16.0 (10)
Ti II	4865.610	1.116	-2.810	1.0	... (11)
Ti II	5129.155	1.892	-1.390	6.4	... (10)
Ti II	5185.902	1.893	-1.350	6.2	8.6 (10)
Ti II	5188.691	1.582	-1.210	23.4	27.1 (10)
Ti II	5226.533	1.566	-1.300	...	20.8 (10)
Ti II	5336.778	1.582	-1.630	8.8	... (11)
Ti II	5381.009	1.566	-1.970	4.1	... (11)
Ti II	5418.752	1.582	-2.110	3.8	... (11)
V II	3267.704	1.071	0.283	46.2	... (13)
V II	3276.117	1.128	0.492	58.9	... (13)
V II	3279.845	2.370	0.010	8.5	... (10)
V II	3298.736	1.128	-0.956	7.2	... (13)
V II	3504.444	1.096	-0.714	8.1	... (13)
V II	3517.296	1.128	-0.208	20.1	... (13)
V II	3530.760	1.071	-0.470	12.6	... (13)
V II	3545.194	1.096	-0.259	18.2	... (13)
V II	3566.168	1.071	-1.201	11.1	... (13)
V II	3592.021	1.096	-0.263	18.2	... (13)
V II	3916.411	1.428	-1.053	4.0	... (13)
V II	3951.960	1.476	-0.784	5.1	... (13)

Table 3. (Continued)

Element	Wavelength (Å)	L.E.P. (eV)	$\log gf$	HD140283	LP625-44	
V II	4023.378	1.805	-0.689	3.9	...	(13)
Cr I	3578.683	0.000	0.409	70.8	...	(3)
Cr I	3593.482	0.000	0.307	68.6	67.7	(3)
Cr I	3908.762	1.004	-1.000	4.2	...	(10)
Cr I	3991.123	2.544	0.252	4.6	...	(10)
Cr I	4254.332	0.000	-0.114	65.9	...	(3)
Cr I	4274.796	0.000	-0.231	61.3	...	(3)
Cr I	4289.716	0.000	-0.361	57.6	...	(3)
Cr I	4337.566	0.968	-1.112	6.0	...	(10)
Cr I	4344.507	1.004	-0.550	9.7	...	(10)
Cr I	4351.051	0.968	-1.449	4.4	...	(10)
Cr I	4526.466	2.544	-0.156	3.4	...	(10)
Cr I	4616.137	0.983	-1.190	4.1	...	(10)
Cr I	4626.188	0.968	-1.320	3.8	...	(10)
Cr I	4652.158	1.004	-1.030	3.8	...	(10)
Cr I	5204.518	0.941	-0.208	...	24.8	(10)
Cr I	5208.437	0.941	0.158	44.6	40.3	(10)
Cr I	5345.807	1.004	-0.980	6.4	...	(10)
Cr I	5348.319	1.004	-1.290	2.7	...	(10)
Cr I	5409.791	1.030	-0.720	10.1	...	(10)
Mn I	3577.870	2.114	0.160	4.3	...	(10)
Mn I	3823.508	2.143	0.058	10.3	...	(10)
Mn I	4030.753	0.000	-0.470	67.5	56.8	(3)
Mn I	4033.062	0.000	-0.618	55.7	50.4	(3)
Mn I	4034.483	0.000	-0.811	47.3	...	(3)
Mn I	4041.357	2.114	0.285	12.4	...	(10)
Mn I	4055.548	2.143	-0.070	5.1	...	(10)
Mn I	4451.575	2.888	0.278	2.6	...	(10)
Mn I	4783.432	2.298	0.042	5.9	...	(10)
Mn I	4823.528	2.319	0.144	6.6	...	(10)
Fe I	3205.398	2.482	-0.340	43.8	...	(14)
Fe I	3210.229	2.425	-0.710	27.7	...	(14)
Fe I	3210.830	2.469	-0.370	40.2	...	(14)
Fe I	3214.396	0.087	-2.620	48.4	...	(14)
Fe I	3215.938	2.469	-0.320	40.4	...	(14)
Fe I	3219.582	2.450	-0.190	47.1	...	(14)

Table 3. (Continued)

Element	Wavelength (Å)	L.E.P. (eV)	$\log gf$	HD140283	LP625-44
Fe I	3222.067	2.399	-0.250	60.8	... (15)
Fe I	3228.249	2.469	-0.760	29.9	... (14)
Fe I	3229.990	3.047	-0.740	21.6	... (14)
Fe I	3230.963	2.450	-0.520	34.6	... (15)
Fe I	3244.188	2.425	-0.270	45.0	... (14)
Fe I	3246.481	2.588	-1.450	4.9	... (14)
Fe I	3246.961	2.198	-1.290	16.4	... (14)
Fe I	3248.204	2.450	-0.670	29.3	... (14)
Fe I	3253.600	3.251	-0.640	7.0	... (14)
Fe I	3257.593	2.176	-1.150	17.6	... (14)
Fe I	3259.990	2.450	-1.370	13.8	... (14)
Fe I	3264.513	2.198	-1.310	11.9	... (14)
Fe I	3265.047	0.087	-3.000	34.0	... (14)
Fe I	3265.617	2.176	-0.610	40.9	... (14)
Fe I	3268.233	2.223	-1.540	9.2	... (14)
Fe I	3276.471	2.198	-1.590	8.3	... (14)
Fe I	3280.260	3.301	-0.130	20.0	... (14)
Fe I	3284.587	2.198	-1.340	14.9	... (14)
Fe I	3288.966	2.198	-1.900	3.7	... (14)
Fe I	3290.988	2.223	-1.210	15.8	... (14)
Fe I	3292.021	3.251	-0.070	19.8	... (14)
Fe I	3292.589	2.223	-0.890	29.7	... (15)
Fe I	3298.132	2.223	-1.130	18.6	... (14)
Fe I	3305.971	2.198	-0.330	52.5	... (14)
Fe I	3307.233	3.237	-0.380	9.3	... (14)
Fe I	3310.342	2.949	-1.170	3.5	... (14)
Fe I	3314.741	3.301	-0.080	17.6	... (14)
Fe I	3317.120	2.279	-1.812	5.6	... (15)
Fe I	3323.737	2.832	-0.600	16.0	... (15)
Fe I	3324.536	2.404	-1.500	7.9	... (14)
Fe I	3325.464	2.453	-1.560	6.3	... (14)
Fe I	3328.866	3.267	-0.390	9.5	... (14)
Fe I	3331.611	2.433	-1.570	6.5	... (14)
Fe I	3335.770	2.845	-1.200	4.8	... (14)
Fe I	3337.666	2.692	-1.040	11.5	... (14)
Fe I	3339.195	2.453	-1.690	4.2	... (14)

Table 3. (Continued)

Element	Wavelength (Å)	L.E.P. (eV)	$\log gf$	HD140283	LP625-44
Fe I	3351.522	2.198	-2.100	5.0	... (14)
Fe I	3351.744	2.728	-1.590	5.4	... (14)
Fe I	3354.060	2.858	-1.170	4.4	... (14)
Fe I	3355.228	3.301	-0.400	11.7	... (14)
Fe I	3356.401	2.279	-1.880	6.7	... (14)
Fe I	3370.783	2.692	-0.270	32.3	... (14)
Fe I	3379.018	2.176	-1.410	15.4	... (14)
Fe I	3380.110	2.759	-0.700	22.8	... (14)
Fe I	3382.402	2.176	-1.910	5.1	... (14)
Fe I	3392.305	2.198	-1.070	21.2	... (14)
Fe I	3392.652	2.176	-0.640	43.0	... (14)
Fe I	3396.976	0.958	-2.430	18.0	... (14)
Fe I	3397.638	0.990	-3.170	5.9	... (14)
Fe I	3399.333	2.198	-0.620	41.2	... (14)
Fe I	3401.519	0.915	-2.060	31.6	... (14)
Fe I	3402.256	3.237	-0.310	17.1	... (14)
Fe I	3406.437	3.274	-0.590	6.8	... (15)
Fe I	3406.800	2.223	-0.960	27.5	... (14)
Fe I	3407.460	2.176	-0.020	63.8	... (14)
Fe I	3410.895	0.915	-3.310	2.3	... (14)
Fe I	3411.353	2.728	-1.060	8.0	... (15)
Fe I	3413.132	2.198	-0.400	47.7	... (14)
Fe I	3415.532	2.223	-1.390	13.0	... (14)
Fe I	3417.841	2.223	-0.680	38.2	... (14)
Fe I	3418.507	2.223	-0.760	34.4	... (14)
Fe I	3424.284	2.176	-0.700	38.5	... (14)
Fe I	3425.010	3.047	-0.500	14.2	... (14)
Fe I	3426.382	0.990	-1.910	36.4	... (14)
Fe I	3427.119	2.176	-0.100	59.8	... (14)
Fe I	3428.193	2.198	-0.820	35.5	... (14)
Fe I	3428.748	3.603	-0.630	5.0	... (15)
Fe I	3442.364	2.279	-1.393	13.9	... (15)
Fe I	3442.669	0.958	-2.660	13.0	... (14)
Fe I	3445.149	2.198	-0.540	44.2	... (14)
Fe I	3447.278	2.198	-1.020	23.4	... (14)
Fe I	3450.328	2.223	-0.900	25.6	... (14)

Table 3. (Continued)

Element	Wavelength (Å)	L.E.P. (eV)	$\log gf$	HD140283	LP625-44
Fe I	3451.614	2.424	-1.560	6.0	... (14)
Fe I	3451.915	2.223	-1.000	26.4	... (14)
Fe I	3452.275	0.958	-1.920	40.5	... (14)
Fe I	3459.427	2.692	-1.630	2.2	... (14)
Fe I	3462.353	2.198	-2.110	2.4	... (15)
Fe I	3463.302	1.485	-2.720	3.2	... (14)
Fe I	3468.845	2.559	-1.290	8.5	... (14)
Fe I	3469.832	2.609	-1.633	3.7	... (15)
Fe I	3476.345	3.603	-0.470	3.2	... (14)
Fe I	3477.853	2.223	-2.120	3.5	... (15)
Fe I	3485.340	2.198	-1.150	22.1	... (14)
Fe I	3512.226	2.851	-1.490	3.0	... (14)
Fe I	3514.628	2.404	-2.020	2.9	... (14)
Fe I	3516.411	3.018	-1.250	5.9	... (15)
Fe I	3518.681	2.876	-1.520	5.8	... (14)
Fe I	3521.261	0.915	-0.990	74.8x	70.0 (14)
Fe I	3522.268	2.833	-0.990	9.4	... (14)
Fe I	3522.900	2.876	-1.340	3.5	... (14)
Fe I	3524.077	2.588	-1.150	11.6	... (15)
Fe I	3524.240	2.279	-1.180	18.6	... (14)
Fe I	3527.793	2.851	-0.440	22.6	... (14)
Fe I	3529.820	2.882	-0.360	...	43.6 (14)
Fe I	3530.387	2.808	-0.950	11.2	... (14)
Fe I	3533.007	2.885	-0.320	25.3	... (14)
Fe I	3533.198	2.882	-0.110	35.3	... (14)
Fe I	3536.556	2.876	0.120	41.0	44.6 (14)
Fe I	3537.493	2.588	-1.530	5.0	... (14)
Fe I	3537.729	2.609	-1.130	10.0	... (14)
Fe I	3537.895	2.833	-0.760	17.8	... (15)
Fe I	3540.121	2.865	-0.790	14.0	... (14)
Fe I	3540.710	0.915	-2.490	17.5	... (14)
Fe I	3541.083	2.851	0.250	45.5	... (14)
Fe I	3542.075	2.865	0.210	44.3	... (14)
Fe I	3543.385	2.433	-1.990	2.2	... (14)
Fe I	3543.674	3.415	-0.770	5.6	... (15)
Fe I	3544.633	2.609	-1.860	2.8	... (15)

Table 3. (Continued)

Element	Wavelength (Å)	L.E.P. (eV)	$\log gf$	HD140283	LP625-44
Fe I	3545.640	2.851	-0.460	20.3	... (14)
Fe I	3547.194	3.301	-0.920	4.9	... (14)
Fe I	3548.020	3.017	-1.260	8.6	... (15)
Fe I	3549.860	1.608	-2.540	6.0	... (15)
Fe I	3553.738	3.573	0.270	20.5	... (14)
Fe I	3554.118	0.958	-2.210	29.7	... (14)
Fe I	3554.501	2.882	-1.030	9.5	... (14)
Fe I	3554.924	2.833	0.540	56.9	... (14)
Fe I	3559.505	3.071	-0.970	6.0	... (15)
Fe I	3564.108	1.608	-2.890	2.6	... (14)
Fe I	3565.379	0.958	-0.130	98.6x	99.5 (14)
Fe I	3567.031	2.876	-0.950	7.8	... (14)
Fe I	3568.434	2.876	-1.520	3.2	... (14)
Fe I	3568.823	3.251	-0.940	4.2	... (14)
Fe I	3568.974	2.692	-1.100	10.0	... (14)
Fe I	3570.099	0.915	0.153	...	125.1 (15)
Fe I	3571.224	1.485	-2.600	6.1	... (15)
Fe I	3573.394	3.301	-0.850	4.4	... (14)
Fe I	3578.382	2.885	-1.350	4.4	... (14)
Fe I	3581.193	0.859	0.406	...	114.3 (15)
Fe I	3581.646	2.692	-1.260	9.6	... (14)
Fe I	3582.200	3.237	-0.300	16.0	... (14)
Fe I	3583.326	3.292	-0.880	8.0	... (15)
Fe I	3584.659	2.692	-0.160	40.5	... (14)
Fe I	3584.958	3.267	0.070	23.6	... (14)
Fe I	3586.112	3.237	0.170	34.6	... (14)
Fe I	3586.739	2.808	-1.040	10.8	... (14)
Fe I	3588.609	2.833	-0.600	21.2	... (14)
Fe I	3588.917	2.876	-0.900	11.1	... (14)
Fe I	3589.105	0.859	-2.115	43.4	28.8 (15)
Fe I	3589.452	2.728	-0.850	15.4	... (14)
Fe I	3594.632	2.851	-0.260	27.8	... (14)
Fe I	3595.301	2.876	-1.100	4.6	... (14)
Fe I	3603.203	2.692	-0.260	32.2	... (14)
Fe I	3606.679	2.692	0.320	59.2	57.0 (14)
Fe I	3608.142	2.851	-0.870	12.6	... (14)

Table 3. (Continued)

Element	Wavelength (Å)	L.E.P. (eV)	$\log gf$	HD140283	LP625-44
Fe I	3608.859	1.011	-0.100	99.4x	94.9 (15)
Fe I	3612.068	2.833	-0.550	18.1	... (14)
Fe I	3613.450	3.251	-1.040	4.1	... (15)
Fe I	3614.772	2.998	-1.440	8.6	... (14)
Fe I	3617.786	3.017	-0.010	30.3	36.4 (14)
Fe I	3621.460	2.728	-0.020	...	41.8 (14)
Fe I	3630.348	2.851	-0.840	8.8	... (14)
Fe I	3631.097	2.833	-0.330	23.9	... (14)
Fe I	3632.039	3.071	-0.180	24.0	... (14)
Fe I	3632.555	2.949	-1.030	7.7	... (15)
Fe I	3634.328	2.940	-0.840	17.4	... (14)
Fe I	3636.994	2.588	-1.460	6.8	... (14)
Fe I	3637.862	2.940	-1.010	8.2	... (15)
Fe I	3638.296	2.759	-0.380	29.6	... (14)
Fe I	3640.388	2.728	-0.110	38.6	38.2 (14)
Fe I	3649.506	2.692	-0.150	...	37.6 (14)
Fe I	3679.913	0.000	-1.599	...	80.0 (3)
Fe I	3685.997	2.940	-0.130	...	36.9 (14)
Fe I	3701.086	2.998	0.070	37.3	29.9 (14)
Fe I	3702.029	2.845	-1.140	13.8	... (15)
Fe I	3709.246	0.915	-0.646	93.3x	92.8 (15)
Fe I	3716.442	2.940	-0.300	26.6	... (14)
Fe I	3718.407	2.759	-1.120	10.1	... (14)
Fe I	3726.926	3.038	-0.320	26.4	... (14)
Fe I	3727.619	0.958	-0.610	92.3x	83.8 (14)
Fe I	3728.668	2.559	-1.610	5.0	... (14)
Fe I	3738.305	3.267	-0.030	29.3	... (14)
Fe I	3740.239	3.251	-0.580	13.3	... (15)
Fe I	3742.617	2.940	-0.890	15.9	25.8 (14)
Fe I	3744.103	3.038	-0.700	14.0	... (14)
Fe I	3745.561	0.087	-0.771	118.8x	117.8 (3)
Fe I	3756.069	2.176	-2.120	4.9	... (14)
Fe I	3756.936	3.573	-0.250	8.7	... (15)
Fe I	3760.049	2.404	-0.847	32.5	... (15)
Fe I	3763.789	0.990	-0.238	103.9x	92.0 (15)
Fe I	3765.539	3.237	0.480	46.3	41.2 (14)

Table 3. (Continued)

Element	Wavelength (Å)	L.E.P. (eV)	$\log gf$	HD140283	LP625-44
Fe I	3766.660	3.038	-1.310	3.3	... (14)
Fe I	3768.028	2.223	-1.640	10.3	... (14)
Fe I	3774.824	2.223	-1.450	17.0	... (14)
Fe I	3776.455	2.176	-1.490	18.2	... (14)
Fe I	3778.315	2.832	-1.850	4.1	... (14)
Fe I	3778.509	3.251	-0.900	6.5	... (14)
Fe I	3781.187	2.198	-1.940	6.3	... (14)
Fe I	3785.948	2.433	-0.940	26.2	... (14)
Fe I	3786.677	1.011	-2.225	35.2	... (15)
Fe I	3787.164	3.640	-0.960	5.0	... (15)
Fe I	3787.880	1.011	-0.859	85.1x	73.6 (15)
Fe I	3789.176	2.728	-1.290	5.3	... (14)
Fe I	3789.820	3.368	-1.230	2.3	... (15)
Fe I	3790.093	0.990	-1.761	56.3	38.8 (15)
Fe I	3790.754	2.176	-1.840	6.6	... (14)
Fe I	3792.155	2.728	-1.430	4.8	... (14)
Fe I	3804.013	3.332	-1.040	5.6	... (15)
Fe I	3805.342	3.301	0.310	39.4	... (14)
Fe I	3806.217	3.415	-0.820	7.6	... (15)
Fe I	3807.537	2.223	-0.990	28.8	... (14)
Fe I	3808.729	2.559	-1.159	14.4	... (15)
Fe I	3809.041	2.858	-1.990	4.3	... (15)
Fe I	3809.564	2.998	-1.550	4.9	... (14)
Fe I	3810.756	3.301	-0.900	6.8	... (14)
Fe I	3811.891	2.759	-1.420	6.6	... (16)
Fe I	3812.964	0.958	-1.010	88.7x	83.0 (16)
Fe I	3816.340	2.198	-1.200	19.2	... (14)
Fe I	3817.640	3.332	-0.700	9.8	... (15)
Fe I	3820.425	0.859	0.119	124.0x	118.5 (15)
Fe I	3821.178	3.267	0.200	40.8	... (14)
Fe I	3821.835	2.609	-1.100	16.1	... (14)
Fe I	3825.881	0.915	-0.037	...	103.1 (15)
Fe I	3827.572	2.692	-1.420	7.0	... (14)
Fe I	3827.823	1.557	0.062	97.5x	84.1 (15)
Fe I	3839.256	3.047	-0.330	25.1	... (14)
Fe I	3840.437	0.990	-0.506	94.9x	84.1 (15)

Table 3. (Continued)

Element	Wavelength (Å)	L.E.P. (eV)	$\log gf$	HD140283	LP625-44
Fe I	3841.048	1.608	-0.065	88.5x	93.0 (16)
Fe I	3843.257	3.047	-0.240	30.9	29.8 (14)
Fe I	3845.169	2.424	-1.390	16.2	... (14)
Fe I	3846.410	3.573	-0.470	12.0	... (14)
Fe I	3850.818	0.990	-1.745	60.0	... (16)
Fe I	3852.573	2.176	-1.180	26.0	... (14)
Fe I	3854.368	3.211	-1.100	5.9	... (14)
Fe I	3856.372	0.052	-1.286	103.2x	93.6 (15)
Fe I	3859.213	2.404	-0.750	36.0	... (14)
Fe I	3859.912	0.000	-0.710	123.2x	116.3 (15)
Fe I	3863.741	2.692	-1.430	7.2	... (14)
Fe I	3867.216	3.017	-0.450	21.6	... (14)
Fe I	3867.920	2.588	-1.850	1.4	... (14)
Fe I	3873.761	2.433	-0.880	36.1	... (14)
Fe I	3878.018	0.958	-0.914	87.3x	85.6 (15)
Fe I	3883.280	3.251	-0.690	13.9	... (14)
Fe I	3885.510	2.424	-1.090	15.1	... (14)
Fe I	3890.840	2.728	-1.310	12.5	... (14)
Fe I	3891.927	3.415	-0.730	8.5	... (14)
Fe I	3897.449	2.949	-1.280	10.2	... (14)
Fe I	3899.707	0.087	-1.531	96.6x	79.8 (15)
Fe I	3902.946	1.557	-0.466	84.4x	69.4 (15)
Fe I	3903.898	2.990	-0.800	20.9	... (14)
Fe I	3906.479	0.110	-2.243	75.5	... (15)
Fe I	3907.934	2.759	-1.120	13.4	... (14)
Fe I	3909.664	3.283	-1.220	3.4	... (15)
Fe I	3910.844	2.759	-1.550	7.1	... (14)
Fe I	3916.731	3.237	-0.600	12.9	... (14)
Fe I	3917.181	0.990	-2.155	41.8	34.4 (15)
Fe I	3918.642	3.018	-0.720	17.0	... (14)
Fe I	3922.912	0.052	-1.651	95.3x	85.0 (15)
Fe I	3925.201	3.292	-1.400	3.7	... (15)
Fe I	3925.644	2.832	-1.030	13.5	16.2 (14)
Fe I	3925.941	2.858	-0.940	...	14.5 (14)
Fe I	3930.297	0.087	-1.490	...	100.7 (14)

Table 3. (Continued)

Element	Wavelength (Å)	L.E.P. (eV)	$\log gf$	HD140283	LP625-44
Fe I	3940.878	0.958	-2.600	24.9	... (15)
Fe I	3941.276	3.266	-1.010	7.6	... (15)
Fe I	3942.440	2.845	-0.950	13.4	... (14)
Fe I	3943.341	2.198	-2.340	4.0	... (14)
Fe I	3944.889	2.990	-1.440	3.1	... (14)
Fe I	3945.117	2.759	-1.460	4.9	... (14)
Fe I	3946.996	3.211	-1.000	4.3	... (14)
Fe I	3947.529	2.832	-1.220	6.2	... (14)
Fe I	3948.096	3.241	-0.560	12.3	... (14)
Fe I	3949.953	2.176	-1.250	25.8	15.6 (14)
Fe I	3951.163	3.274	-0.300	16.3	... (14)
Fe I	3955.342	3.283	-1.010	4.9	... (15)
Fe I	3956.455	3.237	-0.340	22.2	... (14)
Fe I	3956.677	2.692	-0.430	36.1	38.5 (14)
Fe I	3963.101	3.283	-0.700	17.5	... (15)
Fe I	3976.614	3.415	-0.850	13.1	... (14)
Fe I	3977.741	2.198	-1.120	32.4	... (14)
Fe I	3985.387	3.301	-0.990	5.2	... (14)
Fe I	3990.374	3.047	-1.510	3.7	... (14)
Fe I	3994.114	3.047	-1.610	4.3	... (14)
Fe I	3995.983	2.728	-1.570	6.9	... (14)
Fe I	3997.392	2.728	-0.480	34.6	... (14)
Fe I	3998.053	2.692	-0.910	22.1	... (14)
Fe I	4001.661	2.176	-1.900	9.8	... (14)
Fe I	4005.242	1.557	-0.610	79.9x	66.1 (15)
Fe I	4006.311	3.267	-0.990	3.3	... (15)
Fe I	4007.272	2.759	-1.280	7.8	... (14)
Fe I	4009.713	2.223	-1.250	25.6	... (14)
Fe I	4018.268	3.266	-1.230	3.3	... (14)
Fe I	4021.866	2.759	-0.730	24.4	... (14)
Fe I	4024.725	3.241	-0.750	11.6	... (14)
Fe I	4031.960	3.274	-1.060	4.9	... (15)
Fe I	4032.627	1.485	-2.380	10.8	... (14)
Fe I	4043.897	3.241	-0.830	8.1	... (14)
Fe I	4044.609	2.832	-1.220	7.9	... (14)
Fe I	4045.812	1.485	0.280	111.1x	106.4 (15)

Table 3. (Continued)

Element	Wavelength (Å)	L.E.P. (eV)	$\log gf$	HD140283	LP625-44
Fe I	4054.867	3.417	-0.940	6.8	... (15)
Fe I	4062.441	2.845	-0.860	18.5	... (14)
Fe I	4067.271	2.559	-1.419	8.2	... (15)
Fe I	4071.738	1.608	-0.022	91.0x	96.0 (15)
Fe I	4073.763	3.266	-0.900	9.9	... (14)
Fe I	4074.785	3.047	-1.110	10.4	... (14)
Fe I	4076.629	3.211	-0.530	20.4	... (14)
Fe I	4095.970	2.588	-1.480	8.2	... (14)
Fe I	4098.176	3.241	-0.880	5.7	... (14)
Fe I	4109.802	2.845	-0.940	14.1	... (14)
Fe I	4118.545	3.573	0.210	28.0	... (14)
Fe I	4120.207	2.990	-1.270	6.7	... (14)
Fe I	4121.802	2.832	-1.450	7.8	... (14)
Fe I	4122.516	2.845	-1.390	7.8	... (14)
Fe I	4126.183	3.332	-0.960	6.3	... (15)
Fe I	4127.608	2.858	-0.960	13.2	... (14)
Fe I	4132.058	1.608	-0.670	77.2	70.0 (14)
Fe I	4132.899	2.845	-1.010	15.5	... (14)
Fe I	4133.856	3.368	-1.310	4.3	... (14)
Fe I	4134.678	2.832	-0.650	27.3	29.0 (14)
Fe I	4136.998	3.415	-0.450	9.6	... (14)
Fe I	4139.927	0.990	-3.629	4.4	... (15)
Fe I	4143.414	3.047	-0.200	37.3	32.7 (14)
Fe I	4143.868	1.557	-0.510	84.1x	73.4 (14)
Fe I	4147.669	1.485	-2.104	22.5	... (15)
Fe I	4149.365	3.332	-0.850	9.0	... (14)
Fe I	4152.169	0.958	-3.232	10.7	... (15)
Fe I	4153.899	3.397	-0.320	20.2	... (14)
Fe I	4154.499	2.832	-0.690	24.0	... (14)
Fe I	4154.805	3.368	-0.400	18.5	... (14)
Fe I	4156.799	2.832	-0.810	22.6	26.6 (14)
Fe I	4157.779	3.417	-0.400	14.2	... (14)
Fe I	4158.793	3.430	-0.670	6.7	... (15)
Fe I	4173.920	0.990	-3.290	6.5	... (14)
Fe I	4174.913	0.915	-2.969	16.4	... (15)
Fe I	4175.636	2.845	-0.830	20.5	... (14)

Table 3. (Continued)

Element	Wavelength (Å)	L.E.P. (eV)	$\log gf$	HD140283	LP625-44
Fe I	4181.755	2.832	-0.370	41.1	... (14)
Fe I	4182.382	3.017	-1.180	8.1	... (14)
Fe I	4184.892	2.832	-0.870	16.7	... (14)
Fe I	4187.039	2.450	-0.548	45.8	... (15)
Fe I	4187.795	2.425	-0.554	48.6	... (15)
Fe I	4191.430	2.469	-0.670	39.9	28.7 (14)
Fe I	4195.329	3.332	-0.490	15.9	... (14)
Fe I	4196.208	3.397	-0.700	9.0	... (14)
Fe I	4198.634	3.417	-0.780	15.8	... (15)
Fe I	4200.924	3.397	-0.830	8.6	... (14)
Fe I	4202.029	1.485	-0.708	81.4	68.4 (15)
Fe I	4205.539	3.417	-1.430	4.0	... (14)
Fe I	4207.127	2.832	-1.460	4.0	... (15)
Fe I	4213.647	2.845	-1.290	6.7	... (15)
Fe I	4216.184	0.000	-3.356	36.5	... (3)
Fe I	4217.545	3.430	-0.480	12.4	... (14)
Fe I	4220.342	3.071	-1.310	4.3	... (14)
Fe I	4222.213	2.450	-0.967	27.7	... (15)
Fe I	4224.171	3.368	-0.510	13.6	... (14)
Fe I	4225.455	3.417	-0.510	12.7	... (14)
Fe I	4225.956	3.047	-1.410	4.2	... (14)
Fe I	4227.426	3.332	0.270	43.0	... (14)
Fe I	4233.603	2.482	-0.604	43.8	... (15)
Fe I	4235.937	2.425	-0.341	57.9	... (15)
Fe I	4238.810	3.397	-0.230	21.4	... (14)
Fe I	4247.426	3.368	-0.240	22.1	... (14)
Fe I	4248.225	3.071	-1.290	3.1	... (14)
Fe I	4250.119	2.469	-0.405	53.4	... (15)
Fe I	4250.787	1.557	-0.710	77.0	... (14)
Fe I	4260.474	2.399	0.080	76.9	... (14)
Fe I	4266.965	2.728	-1.810	4.6	... (14)
Fe I	4271.153	2.450	-0.349	59.2	... (15)
Fe I	4282.403	2.176	-0.780	45.6	... (14)
Fe I	4291.464	0.052	-4.080	11.6	... (14)
Fe I	4299.235	2.425	-0.410	64.9	... (14)
Fe I	4337.046	1.557	-1.695	34.5	39.6 (15)

Table 3. (Continued)

Element	Wavelength (Å)	L.E.P. (eV)	$\log gf$	HD140283	LP625-44
Fe I	4352.735	2.223	-1.290	25.1	... (14)
Fe I	4367.903	1.608	-2.890	4.4	... (14)
Fe I	4369.771	3.047	-0.800	18.0	... (14)
Fe I	4375.930	0.000	-3.031	54.4	... (3)
Fe I	4383.545	1.485	0.200	114.9x	118.8 (15)
Fe I	4387.892	3.071	-1.520	3.3	... (14)
Fe I	4388.407	3.603	-0.680	6.8	... (14)
Fe I	4404.750	1.557	-0.142	98.8x	83.6 (15)
Fe I	4407.709	2.176	-1.970	10.8	... (14)
Fe I	4408.414	2.198	-1.770	14.2	... (14)
Fe I	4415.123	1.608	-0.615	82.3	... (15)
Fe I	4422.568	2.845	-1.110	10.3	... (14)
Fe I	4427.310	0.052	-2.920	54.4	... (14)
Fe I	4430.614	2.223	-1.659	12.7	... (15)
Fe I	4433.216	3.654	-0.700	6.0	... (15)
Fe I	4442.339	2.198	-1.255	29.7	... (15)
Fe I	4443.194	2.858	-1.040	13.3	... (14)
Fe I	4447.717	2.223	-1.342	25.8	... (15)
Fe I	4454.381	2.832	-1.300	8.0	... (14)
Fe I	4459.118	2.176	-1.279	34.0	... (15)
Fe I	4461.653	0.087	-3.210	40.9	35.2 (15)
Fe I	4466.552	2.832	-0.600	30.4	... (14)
Fe I	4469.375	3.654	-0.480	10.3	... (14)
Fe I	4476.019	2.845	-0.820	26.7	15.1 (14)
Fe I	4484.220	3.603	-0.860	8.2	7.5 (14)
Fe I	4485.671	3.686	-1.020	3.1	... (15)
Fe I	4489.739	0.121	-3.966	8.7	... (15)
Fe I	4494.563	2.198	-1.136	35.3	27.6 (15)
Fe I	4528.614	2.176	-0.822	50.0	... (15)
Fe I	4531.148	1.485	-2.155	21.7	22.3 (15)
Fe I	4602.941	1.485	-2.210	20.3	13.3 (14)
Fe I	4619.287	3.603	-1.120	3.8	... (15)
Fe I	4625.045	3.241	-1.340	3.8	... (15)
Fe I	4632.912	1.608	-2.913	3.9	... (15)
Fe I	4637.503	3.283	-1.390	4.0	... (15)
Fe I	4647.435	2.949	-1.350	7.1	... (14)

Table 3. (Continued)

Element	Wavelength (Å)	L.E.P. (eV)	$\log gf$	HD140283	LP625-44
Fe I	4667.453	3.603	-0.750	6.9	... (14)
Fe I	4678.846	3.603	-0.830	8.2	... (14)
Fe I	4691.411	2.990	-1.520	4.9	... (14)
Fe I	4707.274	3.241	-1.080	7.6	... (15)
Fe I	4710.283	3.018	-1.610	3.0	... (14)
Fe I	4733.591	1.485	-2.990	4.9	... (14)
Fe I	4736.772	3.211	-0.750	14.3	... (14)
Fe I	4741.529	2.832	-1.760	2.2	... (14)
Fe I	4786.807	3.017	-1.610	3.7	... (14)
Fe I	4789.650	3.547	-0.960	4.3	... (14)
Fe I	4871.318	2.865	-0.360	36.9	30.5 (14)
Fe I	4872.138	2.882	-0.570	27.2	24.4 (14)
Fe I	4878.211	2.885	-0.890	...	25.0 (14)
Fe I	4890.755	2.876	-0.390	35.6	42.1 (14)
Fe I	4891.492	2.851	-0.110	49.6	41.7 (14)
Fe I	4903.310	2.882	-0.930	15.8	13.7 (14)
Fe I	4918.994	2.865	-0.340	38.8	31.7 (14)
Fe I	4920.502	2.833	0.070	59.2	62.5 (14)
Fe I	4924.770	2.279	-2.256	4.7	... (16)
Fe I	4938.814	2.876	-1.080	11.3	... (14)
Fe I	4939.687	0.859	-3.340	8.6	... (15)
Fe I	4946.388	3.368	-1.170	4.3	... (15)
Fe I	4957.298	2.851	-0.410	37.1	... (14)
Fe I	4957.597	2.808	0.230	70.6	62.5 (14)
Fe I	4966.088	3.332	-0.870	8.8	... (14)
Fe I	4973.102	3.960	-0.950	2.7	... (15)
Fe I	4978.604	3.984	-0.930	2.1	... (15)
Fe I	4985.253	3.929	-0.560	5.0	... (14)
Fe I	4985.547	2.865	-1.330	5.7	... (14)
Fe I	4994.130	0.915	-2.956	13.0	10.7 (16)
Fe I	5006.119	2.833	-0.610	28.1	23.9 (14)
Fe I	5012.068	0.859	-2.642	33.1	... (15)
Fe I	5014.942	3.943	-0.300	7.7	... (14)
Fe I	5022.236	3.984	-0.530	3.9	... (15)
Fe I	5028.127	3.573	-1.120	2.7	... (14)
Fe I	5041.072	0.958	-3.090	14.6	... (14)

Table 3. (Continued)

Element	Wavelength (Å)	L.E.P. (eV)	$\log gf$	HD140283	LP625-44
Fe I	5041.756	1.485	-2.200	22.2	... (14)
Fe I	5049.820	2.279	-1.344	21.9	... (16)
Fe I	5051.635	0.915	-2.795	24.3	11.8 (15)
Fe I	5074.749	4.220	-0.200	6.5	... (15)
Fe I	5079.224	2.198	-2.067	4.6	... (15)
Fe I	5079.740	0.990	-3.220	6.3	... (15)
Fe I	5083.339	0.958	-2.958	15.7	... (15)
Fe I	5098.697	2.176	-2.030	9.9	... (14)
Fe I	5107.641	1.557	-2.418	39.4	... (15)
Fe I	5110.413	0.000	-3.760	22.6	... (3)
Fe I	5123.720	1.011	-3.068	12.1	... (15)
Fe I	5125.117	4.220	-0.140	7.2	... (15)
Fe I	5127.359	0.915	-3.307	9.6	... (15)
Fe I	5133.689	4.178	0.140	14.3	... (15)
Fe I	5137.382	4.178	-0.400	8.1	... (15)
Fe I	5141.739	2.424	-1.964	4.6	... (16)
Fe I	5142.929	0.958	-3.080	11.3	... (16)
Fe I	5150.839	0.990	-3.003	10.8	... (16)
Fe I	5162.273	4.178	0.020	12.6	... (15)
Fe I	5166.282	0.000	-4.195	9.9	... (15)
Fe I	5171.597	1.485	-1.793	41.7	29.6 (15)
Fe I	5191.455	3.038	-0.550	23.0	... (14)
Fe I	5192.344	2.998	-0.420	29.6	24.5 (14)
Fe I	5194.942	1.557	-2.090	24.9	14.9 (15)
Fe I	5198.711	2.223	-2.135	4.7	... (15)
Fe I	5202.336	2.176	-1.838	12.9	7.8 (15)
Fe I	5204.583	0.087	-4.332	33.8	... (15)
Fe I	5216.274	1.608	-2.150	20.3	13.4 (15)
Fe I	5217.390	3.211	-1.070	6.5	... (16)
Fe I	5225.525	0.110	-4.789	2.2	... (15)
Fe I	5226.862	3.038	-0.550	...	19.9 (14)
Fe I	5227.189	1.557	-1.230	...	52.2 (14)
Fe I	5232.940	2.940	-0.060	48.5	... (14)
Fe I	5263.305	3.266	-0.879	11.1	... (16)
Fe I	5266.555	2.998	-0.390	...	29.1 (14)
Fe I	5269.537	0.859	-1.321	95.6	... (15)

Table 3. (Continued)

Element	Wavelength (Å)	L.E.P. (eV)	$\log gf$	HD140283	LP625-44
Fe I	5283.621	3.241	-0.432	...	18.4 (16)
Fe I	5307.361	1.608	-2.987	5.1	... (15)
Fe I	5324.179	3.211	-0.103	33.5	26.8 (16)
Fe I	5328.039	0.915	-1.466	87.3	70.1 (15)
Fe I	5328.531	1.557	-1.850	35.4	24.4 (14)
Fe I	5332.900	1.557	-2.780	5.6	... (14)
Fe I	5339.930	3.266	-0.647	12.9	... (16)
Fe I	5341.023	1.608	-1.950	28.4	17.9 (14)
Fe I	5364.871	4.446	0.230	8.4	... (14)
Fe I	5367.467	4.415	0.440	11.2	14.1 (14)
Fe I	5369.962	4.371	0.540	14.8	13.7 (14)
Fe I	5371.489	0.958	-1.645	78.9	61.5 (15)
Fe I	5383.369	4.312	0.640	18.2	11.4 (14)
Fe I	5393.167	3.241	-0.715	12.2	... (16)
Fe I	5397.128	0.915	-1.993	63.9	46.5 (15)
Fe I	5400.502	4.371	-0.160	4.1	... (15)
Fe I	5404.152	4.435	0.520	17.9	21.8 (14)
Fe I	5405.775	0.990	-1.844	67.0	47.9 (15)
Fe I	5410.910	4.473	0.400	9.8	... (14)
Fe I	5415.199	4.386	0.640	16.4	21.2 (14)
Fe I	5424.068	4.320	0.520	20.5	... (15)
Fe I	5429.697	0.958	-1.879	68.4	47.9 (15)
Fe I	5434.524	1.011	-2.122	52.4	32.8 (15)
Fe I	5445.042	4.386	-0.020	7.3	... (15)
Fe I	5446.917	0.990	-1.910	68.1	43.5 (14)
Fe I	5455.610	1.011	-2.098	58.0	... (16)
Fe I	5463.276	4.435	0.110	4.6	... (15)
Fe I	5497.516	1.011	-2.849	18.1	... (15)
Fe I	5501.465	0.958	-3.050	14.5	... (14)
Fe I	5506.778	0.990	-2.797	20.8	... (15)
Fe I	5569.618	3.417	-0.540	14.3	19.9 (15)
Fe I	5572.842	3.397	-0.275	20.0	26.1 (16)
Fe I	5576.088	3.430	-1.000	6.3	... (15)
Fe I	5586.755	3.368	-0.096	28.3	... (16)
Fe I	5615.644	3.332	0.050	35.0	... (16)
Fe I	5624.542	3.417	-0.755	8.0	... (16)

Table 3. (Continued)

Element	Wavelength (Å)	L.E.P. (eV)	$\log gf$	HD140283	LP625-44
Fe I	5658.816	3.397	-0.793	6.2	... (16)
Fe I	5662.517	4.178	-0.570	3.0	... (14)
Fe I	5701.543	2.559	-2.216	5.1	... (15)
Fe I	5709.378	3.368	-1.028	6.5	... (16)
Fe I	5762.992	4.209	-0.450	4.2	... (15)
Fe I	6020.173	4.608	-0.270	3.7	... (15)
Fe I	6065.481	2.609	-1.530	10.4	... (15)
Fe I	6136.614	2.453	-1.400	19.8	14.1 (15)
Fe I	6137.691	2.588	-1.403	17.4	11.6 (15)
Fe I	6191.558	2.433	-1.420	16.7	... (14)
Fe I	6213.429	2.223	-2.480	3.3	... (14)
Fe I	6219.280	2.198	-2.433	4.6	... (15)
Fe I	6230.723	2.559	-1.281	19.6	... (15)
Fe I	6246.318	3.603	-0.733	6.0	... (16)
Fe I	6252.555	2.404	-1.687	11.1	... (15)
Fe I	6254.257	2.279	-2.443	4.1	... (16)
Fe I	6335.330	2.198	-2.180	7.9	... (14)
Fe I	6336.835	3.686	-1.050	6.3	... (15)
Fe I	6393.601	2.433	-1.432	16.0	... (16)
Fe I	6546.238	2.759	-1.540	6.5	... (14)
Fe I	6592.913	2.728	-1.470	7.2	... (14)
Fe I	6593.868	2.433	-2.422	2.0	... (15)
Fe I	6663.440	2.424	-2.479	2.4	... (15)
Fe I	7187.317	4.103	-0.150	7.5	... (14)
Fe I	7511.020	4.178	0.100	13.9	... (14)
Fe II	3210.449	1.724	-1.790	78.5x	... (15)
Fe II	3213.310	1.695	-1.310	82.0x	... (17)
Fe II	3231.702	3.892	-1.830	7.8	... (15)
Fe II	3232.791	4.154	-1.440	6.0	... (15)
Fe II	3237.815	3.889	-1.380	16.3	... (15)
Fe II	3243.723	4.149	-1.300	11.0	... (15)
Fe II	3255.884	0.986	-2.500	70.8x	... (15)
Fe II	3258.774	3.892	-1.180	20.9	... (15)
Fe II	3259.052	3.903	-1.040	22.3	... (15)
Fe II	3277.347	0.986	-2.470	76.2x	... (15)
Fe II	3281.293	1.040	-2.690	65.3	... (15)

Table 3. (Continued)

Element	Wavelength (Å)	L.E.P. (eV)	$\log gf$	HD140283	LP625-44
Fe II	3289.347	3.814	-1.620	16.8	... (15)
Fe II	3295.814	1.076	-2.900	52.2	... (15)
Fe II	3302.861	1.040	-3.510	35.1	... (15)
Fe II	3313.996	1.097	-3.930	18.1	... (15)
Fe II	3416.021	2.276	-2.950	13.8	... (15)
Fe II	3425.582	1.671	-3.730	9.3	... (15)
Fe II	3456.928	3.903	-2.280	3.5	... (15)
Fe II	3463.974	1.671	-4.280	4.3	... (15)
Fe II	3468.680	4.154	-1.690	4.5	... (15)
Fe II	3487.990	1.695	-3.890	7.0	... (15)
Fe II	3494.672	2.276	-3.080	10.5	... (15)
Fe II	3507.387	2.342	-3.330	4.0	... (15)
Fe II	3508.213	1.724	-4.210	3.2	... (15)
Fe II	4178.855	2.583	-2.480	17.7	... (15)
Fe II	4233.167	2.583	-2.000	43.2	... (15)
Fe II	4416.817	2.778	-2.600	13.1	... (15)
Fe II	4489.185	2.828	-2.970	5.8	... (15)
Fe II	4491.401	2.856	-2.700	6.4	... (15)
Fe II	4508.283	2.856	-2.580	17.5	13.2 (17)
Fe II	4515.337	2.844	-2.480	13.9	... (15)
Fe II	4520.225	2.807	-2.600	11.1	... (15)
Fe II	4522.634	2.844	-2.030	24.3	... (15)
Fe II	4583.829	2.807	-2.020	...	33.1 (15)
Fe II	4620.513	2.828	-3.290	3.6	... (18)
Fe II	4731.439	2.891	-3.360	5.6	... (15)
Fe II	4923.930	2.891	-1.320	57.8	56.9 (15)
Fe II	5018.450	2.891	-1.220	68.7	66.0 (15)
Fe II	5169.000	2.891	-0.870	...	71.1 (15)
Fe II	5197.559	3.230	-2.100	7.9	... (15)
Fe II	5234.619	3.221	-2.270	13.5	12.6 (18)
Fe II	5275.999	3.199	-1.940	17.3	... (15)
Fe II	5316.624	3.153	-1.850	25.1	31.6 (15)
Fe II	5534.834	3.245	-2.930	4.5	... (15)
Co I	3334.146	0.432	-1.150	16.7	... (19)
Co I	3354.374	0.514	-0.950	14.2	... (15)
Co I	3367.111	0.432	-1.090	14.1	... (15)

Table 3. (Continued)

Element	Wavelength (Å)	L.E.P. (eV)	$\log gf$	HD140283	LP625-44
Co I	3385.219	0.514	-0.950	13.0	... (15)
Co I	3388.163	0.582	-0.790	18.7	... (15)
Co I	3395.370	0.582	-0.400	32.3	... (15)
Co I	3409.177	0.514	-0.230	45.9	... (15)
Co I	3412.339	0.514	0.030	53.4	... (15)
Co I	3412.633	0.000	-0.780	53.6	... (15)
Co I	3417.154	0.582	-0.470	29.4	... (15)
Co I	3431.582	0.101	-0.940	37.1	... (15)
Co I	3433.045	0.629	-0.130	45.3	... (15)
Co I	3442.918	0.174	-1.070	27.1	... (15)
Co I	3443.644	0.514	-0.010	53.1	... (15)
Co I	3449.170	0.582	-0.090	45.3	... (15)
Co I	3449.441	0.432	-0.500	46.7	... (15)
Co I	3455.237	0.224	-1.170	21.3	... (15)
Co I	3462.804	0.629	-0.070	46.7	... (15)
Co I	3483.410	0.514	-1.000	13.2	... (15)
Co I	3489.399	0.923	0.150	37.8	... (15)
Co I	3491.316	0.224	-1.440	17.2	... (15)
Co I	3495.682	0.629	-0.270	43.5	... (15)
Co I	3502.278	0.432	0.070	...	48.1 (15)
Co I	3502.630	0.174	-1.240	30.8	24.5 (15)
Co I	3506.310	0.514	-0.040	60.6	42.3 (15)
Co I	3509.843	0.582	-0.320	37.0	36.5 (15)
Co I	3512.640	0.582	-0.130	44.7	... (15)
Co I	3513.478	0.101	-0.840	45.9	... (15)
Co I	3518.340	1.049	0.070	27.9	... (15)
Co I	3520.075	0.101	-1.290	24.3	... (15)
Co I	3521.567	0.432	-0.580	34.7	... (15)
Co I	3523.423	0.629	-0.440	42.6	... (15)
Co I	3529.032	0.174	-0.880	34.6	20.2 (15)
Co I	3529.816	0.514	-0.070	58.3	41.7 (15)
Co I	3533.356	0.224	-0.990	35.3	31.0 (15)
Co I	3550.592	0.174	-1.520	12.0	5.7 (15)
Co I	3560.891	0.629	-0.760	15.6	... (15)
Co I	3564.947	0.582	-0.970	14.7	10.7 (15)
Co I	3569.370	0.923	0.370	46.3	36.0 (15)

Table 3. (Continued)

Element	Wavelength (Å)	L.E.P. (eV)	$\log gf$	HD140283	LP625-44	
Co I	3574.967	0.582	-0.770	21.3	13.9	(15)
Co I	3575.361	0.101	-0.830	50.2	31.0	(15)
Co I	3578.076	2.280	-0.780	1.7	...	(19)
Co I	3594.870	0.174	-0.970	28.7	28.2	(15)
Co I	3602.079	0.224	-1.110	27.9	...	(15)
Co I	3755.447	2.080	-0.680	5.2	...	(19)
Co I	3842.047	0.923	-0.770	10.6	...	(15)
Co I	3845.468	0.923	0.010	42.8	48.6	(15)
Co I	3873.120	0.432	-0.660	52.7	...	(15)
Co I	3873.953	0.514	-0.870	33.1	...	(15)
Co I	3881.869	0.582	-1.130	17.0	...	(15)
Co I	3894.073	1.049	0.100	39.7	27.0	(15)
Co I	3941.728	0.432	-2.030	4.6	...	(15)
Co I	3995.306	0.923	-0.220	33.2	24.3	(15)
Co I	4020.898	0.432	-2.070	3.3	...	(15)
Co I	4092.386	0.923	-0.940	6.8	10.2	(15)
Co I	4110.532	1.049	-1.080	4.5	...	(15)
Co I	4118.774	1.049	-0.490	18.3	...	(15)
Co I	4121.318	0.923	-0.320	30.9	...	(15)
Ni I	3221.652	0.000	-1.920	53.8	...	(20)
Ni I	3225.020	0.423	-1.404	50.5	...	(20)
Ni I	3310.202	0.423	-3.010	2.2	...	(15)
Ni I	3315.663	0.109	-1.240	65.4	...	(20)
Ni I	3320.257	0.165	-1.432	59.9	...	(20)
Ni I	3322.310	0.423	-1.403	47.5	...	(20)
Ni I	3361.551	0.109	-1.458	60.0	...	(20)
Ni I	3362.806	0.212	-3.570	7.2	...	(20)
Ni I	3365.768	0.423	-1.190	52.9	...	(15)
Ni I	3367.892	0.025	-2.865	15.2	...	(20)
Ni I	3374.221	0.025	-1.760	54.3	...	(15)
Ni I	3380.870	0.275	-1.340	53.7	...	(3)
Ni I	3409.572	0.000	-2.467	28.5	...	(20)
Ni I	3413.472	0.165	-1.480	61.9	...	(3)
Ni I	3413.939	0.109	-1.720	51.4	...	(15)
Ni I	3420.741	0.275	-3.305	3.5	...	(20)
Ni I	3467.502	0.165	-1.980	37.3	...	(15)

Table 3. (Continued)

Element	Wavelength (Å)	L.E.P. (eV)	$\log gf$	HD140283	LP625-44
Ni I	3469.486	0.275	-1.835	42.0	... (20)
Ni I	3483.774	0.275	-1.110	66.8	... (15)
Ni I	3485.888	0.212	-2.150	28.9	... (15)
Ni I	3500.852	0.165	-1.294	65.1	50.1 (20)
Ni I	3502.595	0.000	-2.530	30.8	... (15)
Ni I	3507.694	0.165	-2.510	17.1	... (15)
Ni I	3515.050	0.109	-0.226	...	86.3 (20)
Ni I	3519.759	0.275	-1.422	57.9	... (20)
Ni I	3523.444	0.025	-2.450	42.6	... (15)
Ni I	3524.536	0.025	-0.007	104.1x	92.3 (20)
Ni I	3527.982	0.165	-2.260	29.3	... (15)
Ni I	3548.185	0.212	-1.570	52.5	... (15)
Ni I	3551.526	0.165	-2.700	14.2	... (20)
Ni I	3561.751	0.000	-2.300	23.2	... (15)
Ni I	3566.372	0.423	-0.251	83.6x	73.4 (20)
Ni I	3597.700	0.212	-1.115	68.7	55.0 (20)
Ni I	3602.281	0.165	-2.192	34.1	... (20)
Ni I	3609.314	0.109	-2.090	31.5	22.1 (15)
Ni I	3610.461	0.109	-1.164	69.6	... (20)
Ni I	3612.741	0.275	-1.423	58.0	43.6 (20)
Ni I	3619.392	0.423	0.020	89.0x	82.3 (20)
Ni I	3739.229	0.165	-2.346	13.5	... (20)
Ni I	3775.572	0.423	-1.408	58.5	... (20)
Ni I	3783.530	0.423	-1.310	60.0	... (15)
Ni I	3792.337	0.275	-3.240	4.8	... (15)
Ni I	3807.144	0.423	-1.220	64.3	... (20)
Ni I	3858.301	0.423	-0.951	73.2	68.5 (20)
Ni I	4401.547	3.193	0.080	10.6	... (15)
Ni I	4470.483	3.399	-0.400	2.7	... (15)
Ni I	4604.994	3.480	-0.290	2.9	... (15)
Ni I	4648.659	3.420	-0.160	3.3	... (15)
Ni I	4714.421	3.380	0.230	10.9	... (15)
Ni I	4829.028	3.542	-0.330	2.6	... (15)
Ni I	4831.183	3.606	-0.420	1.7	... (15)
Ni I	4855.414	3.542	0.000	4.3	... (15)
Ni I	4980.161	3.606	-0.110	4.0	... (15)

Table 3. (Continued)

Element	Wavelength (\AA)	L.E.P. (eV)	$\log gf$	HD140283	LP625-44
Ni I	5035.374	3.635	0.290	6.1	... (15)
Ni I	5080.523	3.655	0.130	4.9	... (15)
Ni I	5137.075	1.676	-1.990	8.1	... (15)
Ni I	5476.906	1.826	-0.890	29.8	... (15)
Ni I	6767.778	1.826	-2.170	2.1	... (15)
Sr II	4077.714	0.000	0.150	76.4	139.5 (21)
Sr II	4161.796	2.940	-0.500	...	8.3 (21)
Sr II	4215.524	0.000	-0.180	66.0	115.3 (21)
Y II	3216.680	0.130	-0.020	8.1	... (22)
Y II	3327.876	0.409	0.130	3.9	... (19)
Y II	3549.002	0.130	-0.280	2.5	44.9 (22)
Y II	3600.731	0.180	0.280	10.9	66.7 (22)
Y II	3601.915	0.104	-0.180	6.4	56.8 (22)
Y II	3611.043	0.130	0.010	4.7	55.4 (22)
Y II	3633.121	0.000	-0.080	...	54.2 (22)
Y II	3788.693	0.104	-0.060	5.2	66.9 (22)
Y II	3818.341	0.130	-0.970	...	29.8 (22)
Y II	3950.349	0.104	-0.490	3.3	... (22)
Y II	4177.528	0.409	-0.160	...	58.3 (22)
Y II	4374.933	0.409	0.160	4.9	... (22)
Y II	4854.861	0.992	-0.380	...	23.9 (22)
Y II	4883.682	1.084	0.070	...	31.7 (22)
Y II	5087.418	1.084	-0.160	...	25.8 (22)
Y II	5200.409	0.992	-0.570	...	10.7 (22)
Y II	5205.722	1.033	-0.340	...	17.5 (22)
Zr II	3241.050	0.039	-0.340	5.5	... (23)
Zr II	3279.260	0.095	-0.090	12.3	... (23)
Zr II	3356.090	0.095	-0.420	4.3	... (21)
Zr II	3391.980	0.164	0.530	27.0	... (21)
Zr II	3430.530	0.466	-0.160	3.4	... (19)
Zr II	3438.230	0.095	0.420	23.9	... (21)
Zr II	3457.560	0.559	-0.530	1.6	... (19)
Zr II	3479.390	0.713	0.170	2.3	... (21)
Zr II	3481.150	0.802	0.320	3.3	... (21)
Zr II	3505.670	0.164	-0.360	4.6	... (21)

Table 3. (Continued)

Element	Wavelength (Å)	L.E.P. (eV)	$\log gf$	HD140283	LP625-44	
Zr II	3525.810	0.359	-0.650	...	36.4	(19)
Zr II	3551.950	0.095	-0.310	4.6	65.0	(21)
Zr II	3556.600	0.466	0.140	...	68.3	(19)
Zr II	3573.080	0.319	-1.040	...	34.2	(19)
Zr II	3613.100	0.039	-0.580	...	57.2	(21)
Zr II	3614.770	0.359	-0.250	...	58.3	(19)
Zr II	3630.020	0.359	-1.110	...	25.3	(21)
Zr II	3633.490	1.756	0.360	...	29.9	(23)
Zr II	3998.970	0.559	-0.670	...	44.4	(21)
Zr II	4029.680	0.713	-0.760	...	29.7	(21)
Zr II	4050.330	0.713	-1.000	...	16.9	(21)
Zr II	4149.200	0.802	-0.030	3.9	...	(21)
Zr II	4161.210	0.713	-0.580	...	39.5	(21)
Zr II	4208.980	0.713	-0.460	...	31.8	(21)
Zr II	4443.000	1.486	-0.330	...	14.7	(21)
Zr II	4496.970	0.713	-0.810	...	29.7	(21)
Ba II	4166.003	2.722	-0.410	...	33.1	(2)
Ba II	4524.928	2.512	-0.350	...	50.6	(2)
Ba II	4554.033	0.000	0.163	...	217.0x	(2)
Ba II	4934.086	0.000	-0.160	14.7	212.7x	(2)
Ba II	5853.675	0.604	-1.020	...	106.3	(24)
Ba II	6141.718	0.704	-0.069	...	177.3	(24)
La II	3790.830	0.126	0.143	...	67.1	(25)
La II	3949.100	0.403	0.615	...	137.4	(25)
La II	3988.520	0.403	0.080	...	123.2	(26)
La II	3995.750	0.173	-0.020	...	89.1	(26)
La II	4086.720	0.000	-0.160	...	76.5	(26)
La II	4123.230	0.321	0.120	...	75.3	(26)
La II	4322.510	0.173	-1.050	...	42.6	(25)
La II	4333.740	0.173	-0.160	...	104.8	(26)
La II	4429.900	0.235	-0.370	...	104.6	(25)
La II	4558.460	0.320	-1.020	...	30.8	(25)
La II	4574.880	0.173	-1.120	...	32.2	(25)
La II	4613.390	0.709	-0.467	...	30.9	(25)
La II	4662.510	0.000	-1.280	...	28.0	(25)
Ce II	3529.040	0.709	-0.730	...	21.6	(23)+0.23

Table 3. (Continued)

Element	Wavelength (Å)	L.E.P. (eV)	$\log gf$	HD140283	LP625-44
Ce II	3653.110	0.357	-0.170	...	22.5 (23)+0.23
Ce II	3855.290	0.521	0.000	...	18.9 (23)+0.23
Ce II	3909.310	0.446	-0.520	...	9.9 (23)+0.23
Ce II	3938.090	0.561	-0.090	...	22.3 (23)+0.23
Ce II	3953.950	0.561	-0.660	...	9.0 (23)+0.23
Ce II	3960.910	0.322	-0.200	...	19.0 (23)+0.23
Ce II	3964.500	0.322	-0.500	...	17.9 (23)+0.23
Ce II	3980.880	0.709	0.030	...	17.2 (23)+0.23
Ce II	3984.680	0.956	0.410	...	18.5 (23)+0.23
Ce II	4005.640	0.122	-0.740	...	24.5 (23)+0.23
Ce II	4022.270	1.123	0.050	...	18.0 (23)+0.23
Ce II	4037.670	0.737	-0.190	...	11.8 (23)+0.23
Ce II	4056.900	1.042	-0.490	...	22.9 (23)+0.23
Ce II	4062.220	1.366	0.350	...	19.0 (23)+0.23
Ce II	4072.920	0.328	-0.710	...	24.4 (23)+0.23
Ce II	4117.290	0.740	-0.450	...	8.8 (23)+0.23
Ce II	4153.130	0.232	-0.910	...	15.5 (23)+0.23
Ce II	4185.330	0.417	-0.560	...	15.8 (23)+0.23
Ce II	4444.700	1.058	0.100	...	21.9 (23)+0.23
Ce II	4467.540	0.561	-0.630	...	17.1 (23)+0.23
Ce II	4483.900	0.864	0.090	...	28.1 (23)+0.23
Ce II	4485.520	0.977	-0.720	...	17.9 (23)+0.23
Ce II	4515.860	1.058	-0.520	...	7.9 (23)+0.23
Ce II	4544.960	0.417	-0.890	...	14.5 (23)+0.23
Ce II	4551.300	0.740	-0.490	...	16.9 (23)+0.23
Ce II	4560.960	0.684	-0.470	...	18.2 (23)+0.23
Ce II	4565.840	1.088	0.070	...	20.5 (23)+0.23
Ce II	4606.400	0.910	-0.120	...	22.4 (23)+0.23
Ce II	5187.450	1.212	0.160	...	19.8 (23)+0.23
Ce II	5330.540	0.869	-0.510	...	11.6 (23)+0.23
Ce II	5353.530	0.879	-0.120	...	29.4 (23)+0.23
Ce II	5512.090	1.008	-0.260	...	14.9 (23)+0.23
Pr II	3918.860	0.372	0.260	...	26.4 (23)+0.60
Pr II	3925.470	0.000	-0.330	...	19.0 (27)
Pr II	3964.260	0.216	-0.330	...	26.8 (23)+0.60
Pr II	3964.810	0.055	0.090	...	28.7 (27)

Table 3. (Continued)

Element	Wavelength (Å)	L.E.P. (eV)	$\log gf$	HD140283	LP625-44
Pr II	3965.250	0.204	-0.130	...	25.0 (27)
Pr II	4056.540	0.630	0.640	...	26.8 (23)+0.60
Nd II	3865.980	0.380	-0.800	...	26.2 (19)
Nd II	3981.240	0.205	-1.010	...	14.5 (19)
Nd II	4133.360	0.321	-0.520	...	26.1 (28)
Nd II	4160.570	0.559	-0.450	...	20.1 (19)
Nd II	4368.640	0.064	-0.800	...	17.7 (19)
Nd II	4465.600	0.182	-1.130	...	9.4 (19)
Nd II	4516.360	0.321	-0.750	...	14.5 (19)
Nd II	4542.603	0.742	-0.350	...	20.2 (19)
Nd II	4567.610	0.205	-1.250	...	7.4 (19)
Nd II	4579.320	0.742	-0.550	...	13.6 (19)
Sm II	3922.400	0.378	0.090	...	18.8 (23)+0.49
Sm II	3941.870	0.000	-0.590	...	15.9 (23)+0.49
Sm II	4318.935	0.277	-0.270	...	19.5 (29)
Sm II	4434.320	0.378	-0.260	...	23.0 (23)+0.49
Sm II	4458.520	0.104	-0.780	...	14.7 (23)+0.49
Sm II	4537.954	0.485	-0.230	...	17.4 (29)
Sm II	4543.950	0.333	-0.680	...	15.3 (23)+0.49
Sm II	4552.660	0.248	-1.060	...	6.2 (23)+0.49
Sm II	4566.210	0.333	-0.920	...	18.9 (23)+0.49
Sm II	4595.290	0.485	-0.710	...	8.6 (23)+0.49
Eu II	3907.100	0.207	0.196	...	51.3 (26)
Eu II	6645.110	1.380	0.204	...	7.9 (26)
Gd II	3549.360	0.240	0.260	...	40.6 (30)
Gd II	3656.150	0.144	-0.080	...	35.0 (23)
Gd II	3844.580	0.144	-0.510	...	21.8 (23)
Gd II	3957.670	0.600	-0.260	...	22.2 (30)
Gd II	4037.900	0.556	-0.230	...	19.1 (30)
Gd II	4070.290	0.556	-0.510	...	13.2 (23)
Gd II	4085.560	0.731	0.070	...	17.5 (30)
Dy II	3523.982	0.538	0.480	...	41.2 (31)
Dy II	3531.706	0.000	0.720	...	69.8 (31)
Dy II	3536.019	0.538	0.250	...	40.4 (31)
Dy II	3550.218	0.590	0.290	...	28.3 (31)
Dy II	3788.436	0.103	-0.520	...	19.8 (31)

Table 3. (Continued)

Element	Wavelength (\AA)	L.E.P. (eV)	$\log gf$	HD140283	LP625-44
Dy II	3944.683	0.000	0.075	...	45.7 (31)
Dy II	3996.688	0.590	-0.180	...	18.0 (31)
Dy II	4077.964	0.103	-0.025	...	54.3 (31)
Er II	3559.896	0.000	-0.740	...	29.0 (32)
Er II	3580.519	0.055	-0.770	...	33.9 (32)
Er II	3633.536	0.000	-0.690	...	29.9 (32)
Er II	3786.836	0.000	-0.640	...	42.2 (32)
Er II	3791.829	0.055	-0.060	...	27.4 (32)
Er II	3938.630	0.000	-0.520	...	43.5 (32)
Tm II	3462.200	0.000	-0.350	...	syn (23)
Tm II	3700.260	0.029	-0.770	...	syn (23)
Tm II	3701.360	0.000	-0.890	...	syn (23)
Yb II	3694.200	0.000	-0.230	...	syn (26)
Hf II	3918.090	0.450	-1.260	...	syn (26)
Hf II	4093.160	0.450	-1.390	...	syn (26)
Pb I	3683.462	0.969	-0.520	...	syn (33)
Pb I	4057.815	1.320	-0.200	...	syn (33)

^aThis table is available only in electronic version.

^b Most line data have been compiled in [te\]cite.hirata94Hirata & Horaguchi \(1994\)](#) ([\[cite\]cite.hirata94Hirata & Horaguchi \(1994\)](#)).

References.— (1)[te\]cite.tomkin95Tomkin et al. \(1995\)](#) ([\[cite\]cite.tomkin95Tomkin et al. \(1995\)](#)); (2)[te\]cite.WM80Wiese & Martin \(1980\)](#) ([\[cite\]cite.WM80Wiese & Martin \(1980\)](#)); (3)[te\]cite.morton91Morton \(1991\)](#) ([\[cite\]cite.morton91Morton \(1991\)](#)); (4)[te\]cite.joensson84Jönsson et al. \(1984\)](#) ([\[cite\]cite.joensson84Jönsson et al. \(1984\)](#)); (5)[te\]cite.gigas88Gigas \(1988\)](#) ([\[cite\]cite.gigas88Gigas \(1988\)](#)); (6)[te\]cite.smith87Smith et al. \(1987\)](#) ([\[cite\]cite.smith87Smith et al. \(1987\)](#)); (7)[te\]cite.smith81Smith & Raggett \(1981\)](#) ([\[cite\]cite.smith81Smith & Raggett \(1981\)](#)); (8)[te\]cite.lawler89Lawler & Dakin \(1989\)](#) ([\[cite\]cite.lawler89Lawler & Dakin \(1989\)](#)); (9)[te\]cite.WF75Wiese & Fuhr \(1975\)](#) ([\[cite\]cite.WF75Wiese & Fuhr \(1975\)](#)); (10)[te\]cite.MFW88Martin, Fuhr & Wiese \(1988\)](#) ([\[cite\]cite.MFW88Martin, Fuhr & Wiese \(1988\)](#)); (11)[te\]cite.bizzarri93Bizzarri et al. \(1993\)](#) ([\[cite\]cite.bizzarri93Bizzarri et al. \(1993\)](#)); (12)[te\]cite.savanov90Savanov, Huovelin & Tuominen \(1990\)](#) ([\[cite\]cite.savanov90Savanov, Huovelin & Tuominen \(1990\)](#)); (13)[te\]cite.biemont89aBiémont et al. \(1989a\)](#) ([\[cite\]cite.biemont89aBiémont et al. \(1989a\)](#)); (14)[te\]cite.obrian91O’Brian et al. \(1991\)](#) ([\[cite\]cite.obrian91O’Brian et al. \(1991\)](#)); (15)[te\]cite.fuhr88Fuhr, Martin & Wiese \(1988\)](#) ([\[cite\]cite.fuhr88Fuhr, Martin & Wiese \(1988\)](#)); (16)[te\]cite.bard91Bard, Kock & Kock \(1991\)](#) ([\[cite\]cite.bard91Bard, Kock & Kock \(1991\)](#)); (17)[te\]cite.pauls90Pauls, Grevesse & Huber \(1990\)](#) ([\[cite\]cite.pauls90Pauls, Grevesse & Huber \(1990\)](#)); (18)[te\]cite.HK90Heise & Kock \(1990\)](#) ([\[cite\]cite.HK90Heise & Kock \(1990\)](#)); (19)[te\]cite.CC83Cowley & Corliss \(1983\)](#) ([\[cite\]cite.CC83Cowley & Corliss \(1983\)](#)); (20)[te\]cite.BBPL89Blackwell et al. \(1989\)](#) ([\[cite\]cite.BBPL89Blackwell et al. \(1989\)](#)); (21)[te\]cite.GBHL81Grevesse et al. \(1981\)](#) ([\[cite\]cite.GBHL81Grevesse et al. \(1981\)](#)); (22)[te\]cite.hannaford82Hannaford et al. \(1982\)](#) ([\[cite\]cite.hannaford82Hannaford et al. \(1982\)](#)); (23)[te\]cite.CB62Corliss & Bozman \(1962\)](#) ([\[cite\]cite.CB62Corliss & Bozman \(1962\)](#)); (24)[te\]cite.kastberg93Kastberg et al. \(1993\)](#) ([\[cite\]cite.kastberg93Kastberg et al. \(1993\)](#)); (25)[te\]cite.BBC96Bord, Barisciano & Cowley \(1996\)](#) ([\[cite\]cite.BBC96Bord, Barisciano & Cowley \(1996\)](#)); (26)[te\]cite.snedden96Snedden et al. \(1996\)](#) ([\[cite\]cite.snedden96Snedden et al. \(1996\)](#)); (27)[te\]cite.G91Goly et al. \(1991\)](#) ([\[cite\]cite.G91Goly et al. \(1991\)](#)); (28)[te\]cite.W85Ward et al. \(1985\)](#) ([\[cite\]cite.W85Ward et al. \(1985\)](#)); (29)[te\]cite.biemont89bBiémont et al. \(1989b\)](#) ([\[cite\]cite.biemont89bBiémont et al. \(1989b\)](#)); (30)[te\]cite.bergstrom88Bergström et al. \(1988\)](#) ([\[cite\]cite.bergstrom88Bergström et al. \(1988\)](#)); (31)[te\]cite.kusz92Kusz \(1992\)](#) ([\[cite\]cite.kusz92Kusz \(1992\)](#)); (32)[te\]cite.musiol83Musiol et al. \(1983\)](#) ([\[cite\]cite.musiol83Musiol et al. \(1983\)](#)); (33)[te\]cite.youssef89Youssef & Khalil \(1989\)](#) ([\[cite\]cite.youssef89Youssef & Khalil \(1989\)](#));

Table 4. Abundance Results

Element	HD140283				LP625-44			
	[X/Fe]	log ϵ_{el}	n	σ	[X/Fe]	log ϵ_{el}	n	σ
C (CH, C ₂)	+0.27	6.3		0.20	+2.25	8.1		0.23
N (CN)					+0.95	6.2		0.35
O	+0.91:	7.26:	2		+1.85:	8.00:	2	
Na I	+0.01	3.82	2	0.24	+1.75	5.35	7	0.14
Mg I	+0.17	5.23	8	0.21	+1.12	5.98	4	0.24
Al I	-0.84	3.11	2	0.30	-0.06	3.71	1	0.25
Si I	+0.06	5.10	1	0.27				
K I	+0.48	3.09	2	0.20				
Ca I	+0.22	4.05	25	0.14	+0.35	3.98	5	0.21
Sc II	+0.08	0.66	16	0.21	+0.38	0.76	3	0.34
Ti I	+0.21	2.63	33	0.22	+0.30	2.52	7	0.19
Ti II	+0.23	2.65	96	0.21	+0.36	2.58	15	0.25
V II	+0.02	1.52	13	0.23				
Cr I	-0.24	2.93	18	0.23	-0.21	2.76	3	0.26
Mn I	-0.48	3.47	10	0.21	-0.51	2.30	2	0.27
Fe I ([Fe/H])	-2.58	4.92	494	0.16	-2.72	4.78	102	0.20
Fe II ([Fe/H])	-2.47	5.03	38	0.21	-2.73	4.77	7	0.15
Co I	+0.29	2.68	57	0.28	+0.18	2.37	17	0.19
Ni I	+0.01	3.74	53	0.27	-0.16	3.37	9	0.27
Sr II	-0.16	0.24	2	0.33	+1.12	1.32	3	0.24
Y II	-0.71	-1.00	9	0.22	+1.02	0.53	13	0.22
Zr II	-0.37	0.10	12	0.22	+1.50	1.39	15	0.21
Ba II	-0.98	-1.28	1	0.24	+2.81	2.31	4	0.24
La II					+2.40	0.90	13	0.26
Ce II					+2.22	1.14	33	0.23
Pr II					+2.10	0.18	6	0.26
Nd II					+2.09	0.86	10	0.17
Sm II					+2.03	0.29	10	0.22
Eu II					+1.72	-0.48	2	0.24
Gd II					+2.23	0.60	7	0.17
Dy II					+2.06	0.51	8	0.25
Er II					+2.45	0.70	6	0.27
Tm II					+2.24	-0.33	3	0.27
Yb II					+3.36:	1.60:	1	

Table 4. (Continued)

Element	HD140283				LP625-44			
	[X/Fe]	$\log \epsilon_{\text{el}}$	n	σ	[X/Fe]	$\log \epsilon_{\text{el}}$	n	σ
Hf II					+2.45	0.48	2	0.27
Pb I					+2.6	1.9	2	0.22